

# Evaluation, validation and improvement of the Site Amplification component of the Groningen Risk Model (KEM-02)

Research Question 1 report

Ministry of Economic Affairs and Climate Policy

1 April 2020

**Project** Evaluation, validation and improvement of the Site Amplification component of the Groningen Risk Model (KEM-02)  
**Client** Ministry of Economic Affairs and Climate Policy

**Document** Research Question 1 report  
**Status** Final version  
**Date** 1 April 2020  
**Reference** 110108/20-005.119

**Project code** 110108  
**Project Leader** F. Besseling MSc  
**Project Director** R.A. de Heij MSc

**Author(s)** J. de Greef MSc  
**Checked by** H.J. Lengkeek MSc  
**Approved by** F. Besseling MSc

**Initials**

**Address** Witteveen+Bos Raadgevende ingenieurs B.V.  
Leeuwenbrug 8  
P.O. Box 233  
7400 AE Deventer  
The Netherlands  
+31 570 69 79 11  
[www.witteveenbos.com](http://www.witteveenbos.com)  
CoC 38020751

The Quality management system of Witteveen+Bos has been approved based on ISO 9001.

© Witteveen+Bos

No part of this document may be reproduced and/or published in any form, without prior written permission of Witteveen+Bos, nor may it be used for any work other than that for which it was manufactured without such permission, unless otherwise agreed in writing. Witteveen+Bos does not accept liability for any damage arising out of or related to changing the content of the document provided by Witteveen+Bos.

## TABLE OF CONTENTS

	<b>MANAGEMENT SUMMARY</b>	<b>5</b>
	<b>TECHNICAL SUMMARY</b>	<b>6</b>
<b>1</b>	<b>INTRODUCTION</b>	<b>9</b>
1.1	Background	9
1.2	Scope	10
<b>2</b>	<b>TOPOGRAPHIC AMPLIFICATION</b>	<b>11</b>
2.1	Description of the phenomenon	11
2.2	Literature overview	12
	2.2.1 Research papers	12
	2.2.2 International codes	16
2.3	Synthesis	18
2.4	Conclusions and recommendations	23
2.5	References	24
<b>3</b>	<b>LATERAL SPREADING</b>	<b>26</b>
3.1	Description of the phenomenon	26
3.2	Literature overview	28
3.3	Synthesis	33
	3.3.1 Applicability	33
	3.3.2 Indicative results for Groningen conditions	36
	3.3.3 Liquefaction susceptibility	39
	3.3.4 Combination of methods	41
	3.3.5 Geometrical considerations	45
3.4	Conclusions and recommendations	46
3.5	References	47
	Last page	48

## MANAGEMENT SUMMARY

Gas production from the Groningen field induces earthquakes. To ensure public safety, the operator NAM-executes an extensive Seismic Hazard and Risk Analysis (HRA) program. This program involves analysis of the ground motions and building damage risks caused by these induced earthquakes. An essential part of the HRA model is the local near-surface ground response.

Current project, KEM-02 as part of 'Kenniprogramma Effecten Mijnbouw', aims for an independent evaluation and validation of the ground response component of the HRA. The objective of this first report (of three) in the KEM-02-project is to answer two main questions: i) Is research available indicating that different peak ground accelerations (PGA) associated to surface water bodies (e.g. ditches and canals) can cause additional damage to nearby buildings? ii) Is it possible that for slightly larger events than recorded till date, lateral spreading (e.g. landslide) can occur?

Site amplification effects of surface water bodies and other topographic irregularities are not explicitly addressed in the current HRA of NAM. Existing research methods from literature and safety code standards typically deal with topographic irregularities of substantially larger dimensions than existing in Groningen. Therefore, the applicability of these topographic amplification methods for Groningen is questionable. In addition, topographic amplification interferes with stratigraphic amplification in a non-trivial manner. The measured ground motion recordings from the station network do not allow to derive solid conclusions on the topographic amplification in Groningen.

Hence, Groningen-specific 2D-finite element simulations of the ground response around canals and at artificial dwelling hills are performed. Inputs for these numerical simulations are ground motions from downhole seismic stations and analysed soil profiles typical for Groningen. The amplification generally increases with decreasing shear wave velocity of the top soil. Additional near-slope topographic amplification of peak ground accelerations up to 40 % is calculated by the simulations. The scatter in the simulated amplification level is, however, large. The spatial extent over which topographic irregularities affect surface ground motions is relatively well captured by analytical methods available in codes and literature. Integration of such methods in NPR 9998 for Groningen could be useful, possibly with some Groningen specific modifications. The present study has only addressed effects on PGA. Ground motion intensity measures like spectral acceleration for larger periods or peak ground velocity (PGV) may be less sensitive to small topographic irregularities.

Liquefaction lateral spreading is the lateral movement of sloping, saturated soils caused by earthquake-induced liquefaction. A liquefaction state is reached by repetitive shearing of the granular material during an earthquake. Extensive Groningen-specific studies have been conducted to assess the liquefaction risk in the region, indicating that severe liquefaction is unlikely for earthquakes being slightly larger compared to the events recorded till date. In the present study, however, we do not consider the likelihood of a soil in Groningen to liquefy. Instead, we focus on the effect of liquefaction lateral spreading, given that severe liquefaction occurs.

Several (combinations of) methods from literature to predict lateral spreading displacement magnitudes have been tested for Groningen. A combined method integrating acceleration time history and gently sloping ground conditions is proposed. The proposed method can be used to provide a first quantitative indication of the displacement magnitude, using local soil investigations, geometry data and location-specific seismic hazard. It is found that lateral spreading can only occur in situations where the predicted liquefied layer is horizontally continuous and where its layer thickness is significantly larger than the vertical distance from the slope. Finally, the proposed method yields calculation of horizontal strain levels, which can be used to assess the risk potential of (infra)structural objects due to lateral spreading.

## TECHNICAL SUMMARY

The Netherlands has one of the largest onshore gas fields in the world in Groningen. This gas field has produced for many decades. Associated to the gas extraction activities, induced earthquakes as well as subsidence are occurring. Magnitude and frequency of the earthquakes have been increasing up to mid-2014, and the largest events have caused damage to buildings.

In the NAM Groningen hazard and risk assessment program, site response is embedded in the Ground Motion Model (GMM). The KEM-02-project, as part of 'Kennisprogramma Effecten Mijnbouw', aims for an independent evaluation and validation of the site amplification component of the GMM. The scope of the KEM-02-project comprises 3 research questions. This report presents research question 1, addressing the following two research questions :

- Are research results available indicating that the effect of surface water bodies (ditches, canals) close to building can cause extra damage, caused by the fact they have different PGA's?
- Is it possible that for slightly larger events 'lateral spreading' occurs? This has been observed in the Meuse levees as a result of the Roermond earthquake. If so, what effect can be expected for infrastructures and building in Groningen?

### Topographic amplification near surface water bodies and other topographic irregularities

The effect of surface water bodies, or more general: topographic irregularities, on peak ground acceleration has been addressed in the present study based on combined literature study and numerical simulations. The effect of topographic irregularities on ground motion is not explicitly addressed by the GMM site response model. It cannot be concluded if such effects are covered by the uncertainty range of the GMM and are therefore significant in terms of building damage potential.

Several researchers have studied the phenomenon of topographic amplification. Some of them have proposed analytical methods to deal with topographic amplification in design. Codes and standards, like Eurocode 8, typically address topographic amplification by means of amplification factors on response spectra as function of topography measures. It is however concluded that both results from other research and code provisions are typically dealing with topographic features being substantially larger compared to the typical topographic irregularities observed in Groningen. For this reason the validity of these methods for Groningen could be questioned.

An important complexity related to topographic amplification is formed by the fact that stratigraphic amplification and topographic amplification interfere. This means that if both soil layering and ground surface level vary spatially, the combined effect is non-trivial. Either amplification or de-amplification can be the net result. Moreover, ground motions are subject to inherent variability. As a consequence it is not possible to, based on the available ground motions recordings in Groningen, derive solid conclusions regarding topographic amplification in Groningen. A much denser local grid of surface recording stations would be required to obtain valuable field evidence indicating if this phenomenon could be significant or not.

For these reasons Groningen specific numerical simulations have been performed within the scope of the present project. 2D-finite element simulations of ground response around canals and at artificial dwelling hills (wierden) are performed. Input ground motions have been derived from the 50 m depth G-stations available in the field and a number of typical Groningen soil profiles have been analysed. Simulation results indicate that the spatial extent over which topographic irregularities affect surface ground motions is relatively well captured by analytical methods available in codes and literature. In addition, the results point out that significant topographic amplification of peak ground accelerations (up to 40 % compared to free field conditions) can occur in close vicinity of slopes with a height disregarded by EN1998-5. The scatter in absolute (de)amplification levels however is large and too little data is available to substantiate which method from literature performs best for Groningen. From a perspective of a balance between simplicity and accuracy the method proposed by Bouckovalas & Papadimitriou (2005) could be useful, possibly with some Groningen specific modifications.

It is noted that in the present study (following the request for offer) the impact of topographic irregularities on peak ground accelerations (PGA) is assessed. PGA is a ground motion intensity measure that is sensitive to high frequency content of ground motions. This makes PGA sensitive to small topographic irregularities. Ground motion intensity measures that are typically used for hazard and risk or damage assessments, like spectral acceleration for larger periods or peak ground velocity (PGV) may be less sensitive to small topographic irregularities. Results for other intensity measure, like peak ground velocity or spectral accelerations, could with limited additional effort be extracted from the simulations performed.

### Lateral spreading

Kramer (2013) provides the following definition of lateral spreading: *Lateral spreading is the finite, lateral movement of gently to steeply sloping, saturated soil deposits caused by earthquake-induced liquefaction.* It is important to emphasize that the precondition for lateral spreading to occur, is earthquake-induced liquefaction. Several definitions of liquefaction exist, but in general it is described as the state in which a saturated granular material has negligible stiffness and strength, comparable to a thick fluid. This state can be reached by repetitive shearing of the granular material during an earthquake.

In the present study we do not consider the likelihood of a soil in Groningen liquefying. Instead we will focus on quantification of the effect of lateral spreading, given that it occurs. For the assessment of liquefaction potential we use the Groningen-specific assessment procedure developed by Green et al. (2018) that is also incorporated in the NPR9998. An indicative overview of the presence of loosely packed sands in the shallow Groningen subsurface can be found in [ref. 18], findings and discussion on what earthquake magnitude is needed to induce liquefaction can be found in [ref. 12] and findings on the likelihood of surficial liquefaction manifestations in Groningen can be found in [ref. 11]. **The results of these studies by Green et al. indicate that large scale liquefaction is unlikely for earthquake events being slightly larger compared to the events recorded till date.**

In general methods available in international literature to predict lateral spreading displacement magnitudes are semi-empirical relations that are substantiated by case history data from tectonic earthquakes. The functional form hereof can lead to significantly larger displacement than is likely for induced earthquakes in Groningen. The present study has evaluated expressions for lateral spreading displacement from different researchers. **A method that accounts for acceleration time history rather than magnitude  $M$  and epicentral distance  $R$  is considered to be more appropriate for Groningen due to the different nature of tectonic and induced earthquakes.** Moreover, we require that the method can also be used for finite slopes with a given free face height. Integrating this based on equal-displacement relations results in 'new' combined methods. Methods and combinations of methods subsequently have been tested for Groningen based on a case studies. A combined method integrating Hamada (1999) and Zhang et al. (2004) is proposed to be applied for Groningen. The main reasons why we suggest specifically this method are consistency of predicted values at short distances from the slope and outcome sensitivity with respect to an often uncertain fines content.

For situations where, following the method by Green et al. (2018), the predicted liquefied layer thickness  $H_{liq}$  is significant and continuous in horizontal direction, there is no indication that lateral spreading cannot occur in Groningen. The proposed expression can be used to provide a first quantitative indication of the displacement magnitude, using local soil investigations, geometry data and location specific seismic hazard. As the horizontal displacement is expressed as a function of the distance from the free face, it is possible to establish horizontal strain levels. To assess risks for foundations and (infra-)structural objects related to lateral spreading, it is recommended to couple these strains to the performance of these objects. This can be combined with a region-wide assessment of the relevance of lateral spreading, by zooming in on locations where significant lateral spreading displacements are calculated.

One additional key aspect for lateral spreading potential is the vertical position of the liquefied layer(s) relative to the free face height. A simple provision from literature is provided in the present report, which may prove very helpful when assessing the many ditches and canals in Groningen that have a relatively small free face height.



# 1

## INTRODUCTION

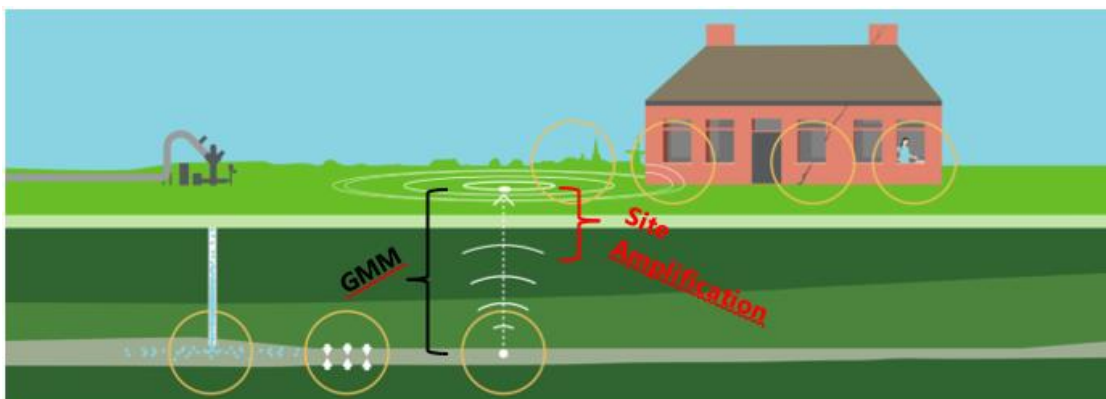
### 1.1 Background

Natural gas in the Netherlands is produced in many onshore and offshore gas fields. The Netherlands has one of the largest onshore gas fields in the world located in Groningen. This gas field has produced for many decades. Associated to the gas extraction activities, induced earthquakes as well as subsidence are occurring. Magnitude and frequency of the earthquakes has been increasing up to midst 2014, and the largest events have caused damage to buildings. The observed damage patterns and ground motions are spatially strongly variable and difficult to forecast. This is a fact difficult to explain to the public and raised during the knowledge platform meetings with the Ministry of Economic Affairs and Climate Policy and the National Coordinator for Groningen. Consequently this had led to the formulation of several research projects within the Knowledge Programme on Effects of Mining (KEM). In this report research question 1 of the KEM-02-project is addressed.

In the NAM Groningen seismic hazard and risk assessment, several topics are addressed from site to source to be able to relate production scenarios to life safety. In figure 1.1 the topics are indicated schematically from left to right using circles: gas production, reservoir compaction, seismology, ground motion prediction, exposure, building strength, building damage. The NAM-ground motion model (GMM) relates the seismological activity in the reservoir layer at a depth of 3,000 meters, to the resulting ground motions that are predicted at surface level. The scope of the KEM-02-project is on the site amplification component of the GMM, which comprises (approximately) the upper 800 meters of the GMM.

The scope of research question 1 in relation to the overall scope of the KEM-02-project, is discussed in the following paragraph.

Figure 1.1 Schematic overview of the site to source assessment path. The NAM-ground motion model (GMM) covers the full extent from the reservoir layer at a depth of 3,000 meters, to ground surface level. The site amplification component comprises (approximately) the upper 800 meters below ground surface level



\* Image: NAM. 2018. Presentation: Seismic Hazard and Risk Assessment in Groningen - Symposium on seismicity induced by gas production from the Groningen Field. <https://www.nam.nl/feiten-en-cijfers/onderzoeksrapporten>.

## 1.2 Scope

The scope of research question 1 as described by the Client in the Request for Offer is:

'Based on literature review and comparison with other such models worldwide for natural or induced earthquakes, assess to what extent the existing model is state of the art and describes its strengths and weaknesses. This evaluation should specifically address the following concerns raised in the past:

- The response of the Froombosch earthquake deviates from other earthquake signatures by its relatively high peak ground acceleration (PGA). Does site response offer an explanation?
- In the Groningen area the subsurface contains a.o. heavy sea clay ('knipklei'), which can contain over-pressured groundwater. Is this adequately represented in the existing model? Is there a specific relationship known or under development between earthquake - knipklei/site response - damage?
- Are research results available indicating that the effect of surface water bodies (ditches, canals) close to buildings can cause extra damage, caused by the fact they have different PGA's?
- Is it possible that for slightly larger events 'lateral spreading' occurs? This has been observed in the Meuse levees as a result of the Roermond earthquake. If so, what effect can be expected for infrastructures and building in Groningen?'

The general focus of the KEM-02-project is on the fundamental understanding of the capabilities and limitations of the site amplification component of the GMM. The deviating response of the Froombosch earthquake directly relates to this understanding and will therefore be addressed under research question 2. The effect of surface water bodies close to buildings also relates to site amplification. However, as will be explained in paragraph 2.1 this phenomenon (called topographic amplification) is not included in the GMM and therefore its possible relevance is discussed separately in the present study. The phenomenon of lateral spreading is not related to the fundamental understanding of site amplification, but nonetheless a concern that needs to be addressed.

The possible effects and presence of knipklei in the Groningen subsurface, are not specifically accounted for in the existing site response model. Significant efforts have been made to acquire the background information report that has led to the concern of the effect of knipklei on the site response. Unfortunately, these efforts have only led to acquiring the review letters by GeoDelft (currently Deltares) and NITG-TNO (currently TNO) dated March 2004. Without access to the background information report itself, we have not been able to review the knipklei properties, presence and thereby its possible relevance to site response.

In the remainder of this report the subject of knipklei/expansive clays is omitted. In chapter 2 the possible effects of topographic amplification are addressed and chapter 3 addresses the possible occurrence and effects of lateral spreading for Groningen conditions.

# 2

## TOPOGRAPHIC AMPLIFICATION

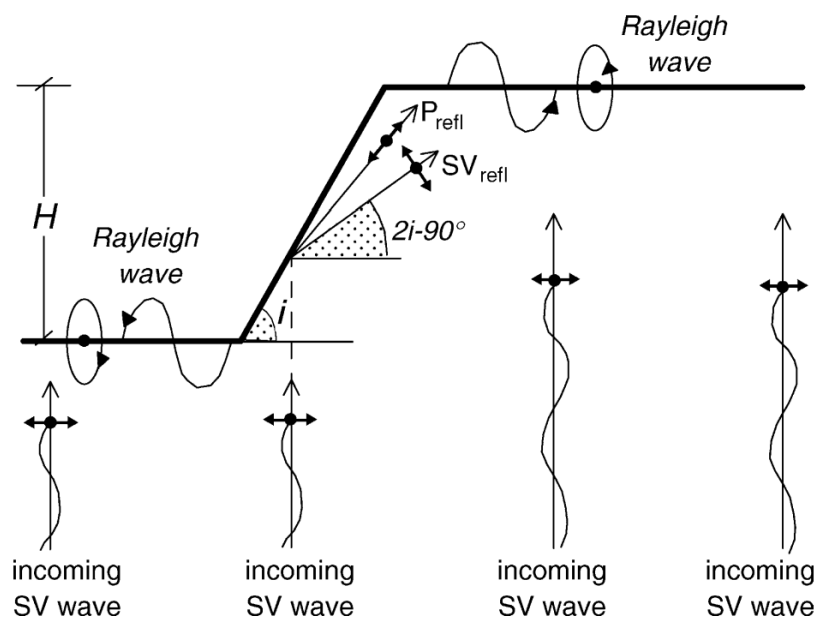
### 2.1 Description of the phenomenon

In the GMM, site amplification is considered from the perspective of vertically propagating shear waves in a 1D-soil column. This implies that for analysis purposes, at every location the implicit assumption is made that the subsurface consists of layers with a certain thickness, that extend infinitely in horizontal direction. The effects of geometric- or topographic irregularities are by definition not captured by performing 1D-site response analyses as the mentioned assumption no longer holds.

The cause of near-slope amplification effects can be attributed to wave reflections that are schematically illustrated in figure 2.1. Herein:

- SV-waves are shear vertical waves: the particle motion of these waves is perpendicular (in the plane of interest) to the direction of wave propagation.
- P-waves are pressure waves: the particle motion of these waves is in this same direction as the wave propagation.
- Rayleigh waves are surface waves: they are created at the surface boundary by a combination of P-waves and SV-waves and the particle motion is rotational with respect to the direction of wave propagation.
- SH-waves (not shown in figure 2.1, but referred to later) are shear horizontal waves: the particle motion of these waves is perpendicular (out of plane) to the direction of wave propagation.

Figure 2.1 Schematic illustration of incoming SV-waves and induced reflected P, SV and Rayleigh waves [ref. 4]



Vertically propagating SV-waves are reflected at the slope leading to a combination of reflected P- and SV-waves and Rayleigh waves. The following cumulative effects of these wave reflections are of engineering interest:

- From purely horizontal motion significant vertical (parasitic) motion is created in the vicinity of the slope.
- In the vicinity of the slope the horizontal motion may be amplified compared to the free field conditions.

In paragraph 2.2 a literature overview on the mechanism, typical findings and recommendations are provided. In paragraph 2.3 some Groningen-specific results based on an earlier study by Witteveen+Bos [ref. 6] are presented and these results are compared with the findings from the literature study. Paragraph 2.4 finalizes the chapter by providing the main conclusions and recommendations.

## 2.2 Literature overview

### 2.2.1 Research papers

Since the early 1970s various studies on the effect of topography on earthquake ground motion have been performed of which Geli et al. (1988) provide a brief review. Herein a distinction is made between the theoretical results obtained from models of varying complexity and field observations/measurements. The main observations and conclusions from the literature review are:

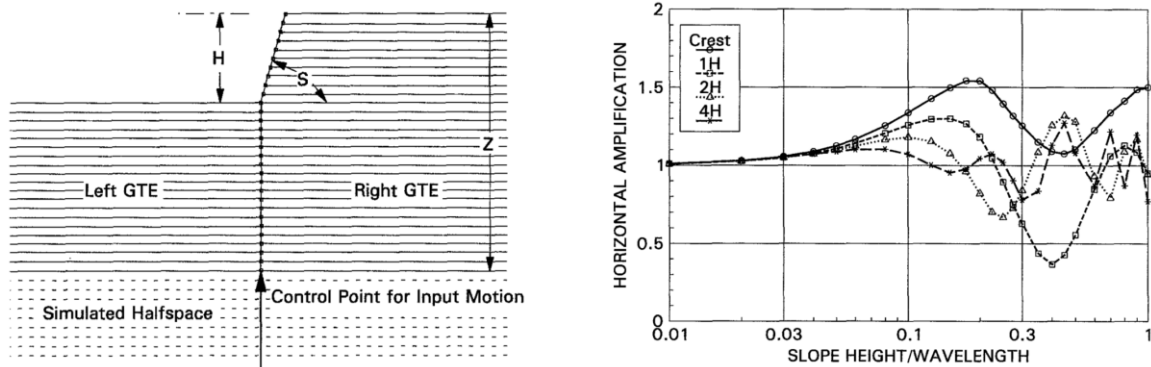
- Qualitatively theory and observations are in agreement for predicting the occurrence of amplification of seismic motion.
- The observed amplification frequency can be predicted well.
- In general the theoretically predicted amplifications are lower than observed values.

After this brief review Geli et al. (1988) also perform multiple time-domain analyses. Herein the response of different subsurface ridge layering configurations to incident SH-waves is investigated. The results from the analyses by Geli et al. (1988) are in qualitative agreement with the conclusions from their literature review, emphasizing that the topographic effect alone is difficult to isolate with respect to other effects such as surface layering and geomorphologically complex structures.

Ashford et al. (1997) note that most research until then has focused on ridges, being significantly different from slopes in the sense that behind the slope crest the soil continues semi-indefinitely. They focus mainly on relative steep slopes and perform a frequency-domain parametric study addressing vertically propagating SH- and SV-waves, the influence of varying slope angles and the relative importance of topographic- and natural (or stratigraphic) soil amplification. The main observations and conclusions are:

- The response at the crest is decreased by increased damping, but the amplification at the crest compared to the free field behind the crest is relatively unaffected by the amount of damping.
- The topographic amplification is higher for SV-waves than for SH-waves.
- The peak topographic amplification occurs at  $H/\lambda$  equal to approximately 0.2, where  $H$  is the slope height and  $\lambda$  is the predominant wavelength of the input motion.
- The topographic amplification tends to increase with increasing slope angle.

Figure 2.2 Left: model representation of a stepped layer on top of a half space. Right: horizontal amplifications for vertically incident SV-wave on a stepped half-space for various distances behind the crest [ref. 2]



By performing an analysis with a stepped layer with thickness  $Z$  on top of a half-space, the relative contributions of natural- and topographic amplification are investigated. Natural (or stratigraphic) amplification is the 1D-site amplification that is caused by combined properties of the input motion and subsurface layers (or stratigraphy), whereas topographic amplification is the additional amplification due to the presence of a slope. Ashford et al. (1997) depict the amplification of motion between any location of interest and the control point for input of motion (see figure 2.2) as the transfer function  $T$ .

To investigate these relative contributions, the thickness  $Z$  of the stepped layer is varied to obtain a range of natural frequencies  $f_n (= V_s/4Z)$  while the topographic frequency  $f_t (\approx V_s/5H)$  remains constant (herein  $V_s$  is the shear wave velocity of the material in m/s). By evaluating the transfer functions at the crest and free field,

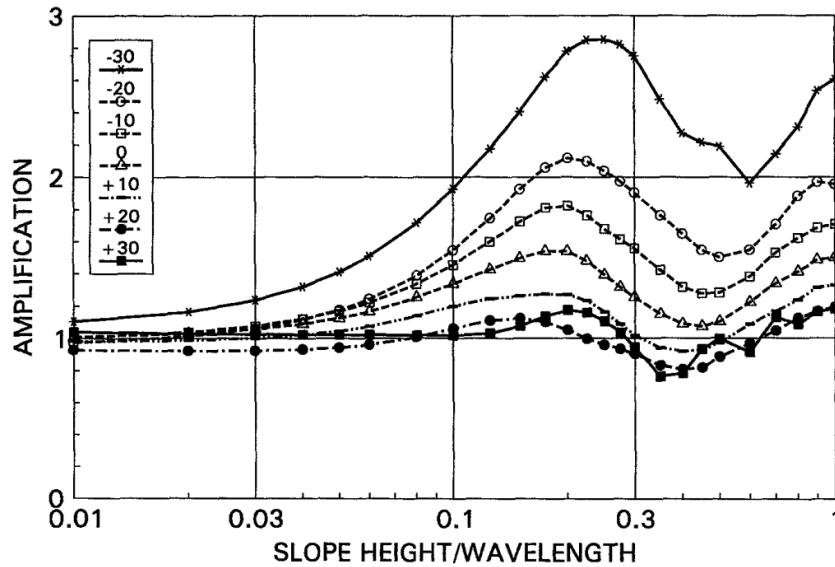
Table 2.1 Transfer functions  $T$  for stepped layer over half-space [ref. 2]

$Z/H$	$f_n$ (Hz)	$f_t$ (Hz)	at the Crest		at Free Field	
			$T_{fn}$	$T_{ft}$	$T_{fn}$	$T_{ft}$
1.00	2.50	2.0	5.2	4.3	2.9	2.2
1.30	1.92	2.0	5.0	4.8	2.9	2.8
1.60	1.56	2.0	4.9	3.0	3.0	1.9
2.00	1.25	2.0	4.3	2.6	3.0	1.2
3.00	0.83	2.0	3.3	1.6	2.9	1.2
4.00	0.62	2.0	3.0	2.1	2.8	2.1
5.00	0.50	2.0	3.0	2.3	2.8	1.0

When the slope height is small compared to the natural frequency wavelength, thus as  $f_n/f_t$  is small, the transfer functions  $T_{fn}$  at the crest and free field are approximately equal. As the natural frequency approaches the topographic frequency at 2.0 Hz, the amplification at the crest increases by over 50 %. From these results Ashford et al. (1997) suggest that the effects of natural- and topographic amplification may work independently.

Ashford & Sitar (1997) investigate the effect of varying inclinations of the incoming SV-waves in frequency-domain parametric analyses, using the same half-space model. As can be seen in figure 2.3 the horizontal amplification is clearly strongly affected by the angle of inclination.

Figure 2.3 Horizontal amplification at the crest for inclined SV-waves on a stepped half-space for various inclination angles [ref. 1].  
Note that the triangular dotted curve highlighting the 0° inclination results equals the Crest curve from figure 2.2



On the basis of a time-domain analysis of a case study Ashford & Sitar (1997) conclude that although the effect of topographic amplification on the horizontal response may be larger for inclined waves, the absolute magnitude of the acceleration is generally largest for the case of vertically propagating waves. The given explanation is that the increased topographic amplification is offset by the reduced site amplification.

Bouckovalas & Papadimitriou (2005, 2006) continue on this topic and include hysteretic damping and the shaking duration in a finite difference modelling approach. The seismic loading is introduced at the base of the model using a time history of stresses to avoid artificial wave reflections at the base. The main observations and conclusions are:

- Slope topography alters mainly the peak acceleration and to a lesser extent the frequency content of horizontal motion.
- Even with only horizontal input motion of SV-waves a parasitic vertical motion is introduced.
- Topography effects fluctuate very strongly with varying distance from the slope, which means verification of results with measurements requires a very dense measurement grid.
- Existing code provisions are in general adequate with respect to the amplification factor, but in general inadequate when it comes to horizontal distances at which these should be applied. In addition, existing codes do not acknowledge the vertical parasitic motion.

Based on their results Bouckovalas & Papadimitriou (2006) make a tentative proposal for code provisions is made to determine topography aggravation factors which should be multiplied with the elastic design response spectrum. These equations are a slightly simplified modification of the equations presented in Bouckovalas & Papadimitriou (2005).

$$S_{hT} = \left\{ \begin{array}{ll} 1.1 + \frac{A_{h,max} - 1.1}{B}(x + B) & , \quad x \leq 0 \\ A_{h,max} & , \quad 0 \leq x \leq 0.2D \\ A_{h,max} - \frac{A_{h,max} - 1.1}{0.8D}(x - 0.2D) & , \quad 0.2D \leq x \end{array} \right\} \geq 1.0$$

$$S_{vT} = \left\{ \begin{array}{ll} 0.1 + \frac{A_{v,max} - 0.1}{0.2D}(x + B + 0.2D) & , \quad x \leq -B \\ A_{v,max} & , \quad -B \leq x \leq 0.2D \\ A_{v,max} - \frac{A_{v,max} - 0.1}{0.5D}(x - 0.2D) & , \quad 0.2D \leq x \end{array} \right\} \geq 0.0$$

Herein  $B$  is the horizontal projected width of the slope,  $x = 0$  is located at the crest of the slope, the positive  $x$  values represent the up-slope direction and the negative  $x$  values the down-slope direction (see figure 2.4). The definitions of  $A_{h,max}$ ,  $A_{v,max}$  and the ratio  $D/H$  are furthermore given by:

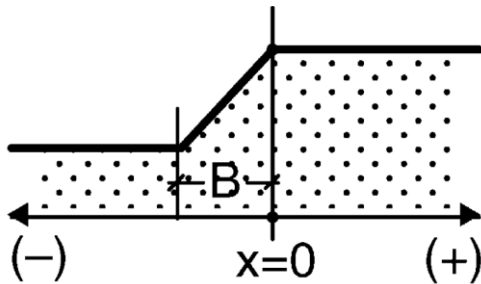
$$A_{h,max} = 1 + 0.2(H/\lambda)^{0.4} \left( \frac{I^2 + 2I^6}{I^3 + 0.02} \right) \quad A_{v,max} = 0.7(H/\lambda)^{0.8} (I^{0.5} + 1.5I^5)$$

$$D/H = 2 \left[ \frac{(H/\lambda)}{(H/\lambda)^2 + 0.2} \right] \left( \frac{I^{1.5} + 3.3I^8}{I^4 + 0.07} \right) \quad I = i/90^\circ$$

Herein  $D$  is the up-slope distance to free-field conditions (i.e. the topographic aggravation becomes negligible), and the definition of the slope angle  $i$  is given in figure 2.1.

Nguyen (2015) based on a numerical parametric study gives similar recommendations, using the same input parameters, although in his study the non-dimensional frequency  $\eta$  is used rather than  $\lambda$ , but this too is a function of the predominant wavelength, given that  $V_s$  is constant. Assessment of the considerations and analysis procedure is difficult as the PhD thesis is written in French and the mentioned journal publications could not be found online.

Figure 2.4 Projected slope width  $B$  and positive/negative  $x$  directions [ref. 4]



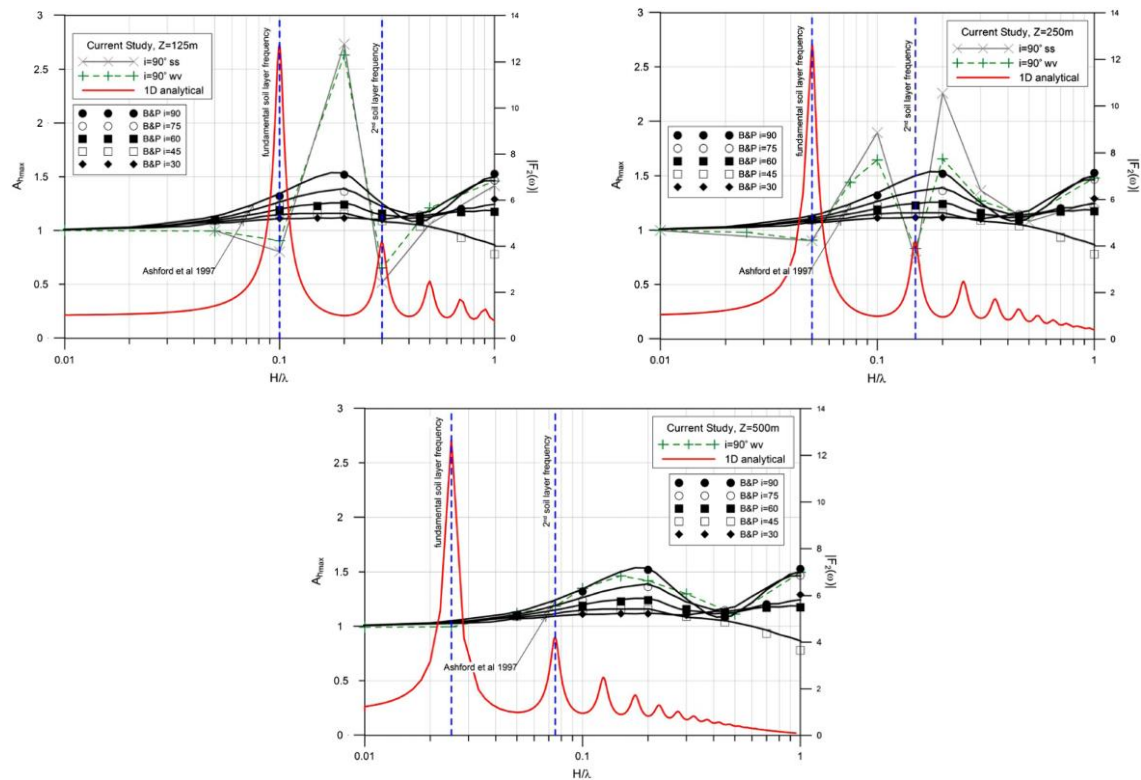
Both of the above studies seem to acknowledge the findings by Ashford et al. (1997) that the topographic amplification can be seen separately from stratigraphic amplification, as the amplification factors are to be multiplied with the ordinates of the elastic response spectrum.

Tripe et al. (2013) introduce a rigid bedrock bottom in their analysis to include the effect of stratigraphic amplification in a time-domain finite element analysis using a sinusoidal time history to obtain the steady state response and Gabor wavelets to mimic earthquake events. Their results are summarized by the densely packed graphs presented in figure 2.5. Herein the normalized horizontal accelerations  $A_{h,max}$  are plotted. These are defined as the ratio of the maximum horizontal accelerations at surface level  $a_{max}$  between the crest and at free-field conditions.

- It can be observed that topographic de-amplification occurs at the natural frequencies of the soil layer.
- The largest topographical amplification occurs not necessarily at  $H/\lambda \approx 0.2$ , but when the normalised frequency of input is between the values corresponding to the natural frequencies of the soil.
- The difference between the steady state (ss) and wavelet (wv) outcomes are small.
- As the bedrock depth increases (lowest plot in figure 2.5,  $Z = 500\text{m}$ ) the outcome appears to approach the homogeneous soil outcomes by Ashford et al. (1997) and Bouckovalas & Papadimitriou (2005). Two possible reasons for this behaviour are given:
  - The topographic effects are reduced as gradually the homogenic half-space case is approached.
  - The natural frequencies are out of the range at which significant topographic effects occur.

The conclusion of the study is that the natural frequency of the soil has a significant, yet complex impact on topographic aggravation. This implies that the contributions of natural site- and topographic amplification cannot be treated separately.

Figure 2.5 Normalized horizontal accelerations at the slope crest for  $Z = 125, 250, 500\text{m}$  [ref. 19]. Included in the figures are the results by Ashford et al. (1997), Bouckovalas & Papadimitriou (2005) and the analytical 1D-stratigraphic amplification



Rizzitano et al. (2014) confirm these conclusions by performing an elaborate parametric study, focussing on the effect of the impedance ratio and soil non-linearity on the topographic amplification. Distinction is made between homogeneous half-space or linear visco-elastic (LVE) models, linear visco-elastic compliant bedrock models (LVEB) and linear visco-elastic rigid bedrock (LVERB) models. These models respectively correspond to impedance ratios  $I_R = (\gamma/V_s)/(\gamma_b/V_{s,b})$  of 1, values between 0 and 1, and 0. The study by Ashford et al. (1997) and Bouckovalas & Papadimitriou (2005) considered the case where  $I_R = 1$  thus neglecting any impedance and Tripe et al. (2013) considered the case where  $I_R = 0$ . Rizzitano et al. (2014) conclude that the impedance ratio has an influence on the total seismic response of the slope, which can be attributed mainly to differences in stratigraphic amplification.

By performing analyses with an equivalent-linear model to account for soil non-linearity, Rizzitano et al. (2014) conclude that non-linear soil behaviour has an effect on topographic amplification. The degree of soil non-linearity depends on, amongst others, the definition of the backbone curves, input motion characteristics and the non-linear stress-strain relationship.

## 2.2.2 International codes

Internationally several codes and guidelines give provisions on how to account for the effects of topographic amplification. Although not all of them have been accessed directly, through other literature a short overview of these provisions is presented.

When assessing the seismic slope stability in the vicinity of structure foundations, EN 1998-5 states in 4.1.3.2(2) that topographic amplification should be accounted for at all structures with an importance factor  $\gamma_I > 1$ . With reference to NPR 9998 [ref. 13] this implies all buildings that fall in consequences class CC2 and higher and in addition new buildings that fall in CC1b. For specification of a factor by which topographic amplification can be accounted, EN 1998-5 makes reference to the (informative) appendix A. Herein the simplified assumption is made that the amplification factor can be applied independently of the fundamental

period of vibration of the subsoil. The ordinates of the elastic response spectrum from EN 1998-1 can therefore be multiplied with a constant amplification factor  $S_T$ . The magnitude and applicability of  $S_T$  is defined from the following criteria:

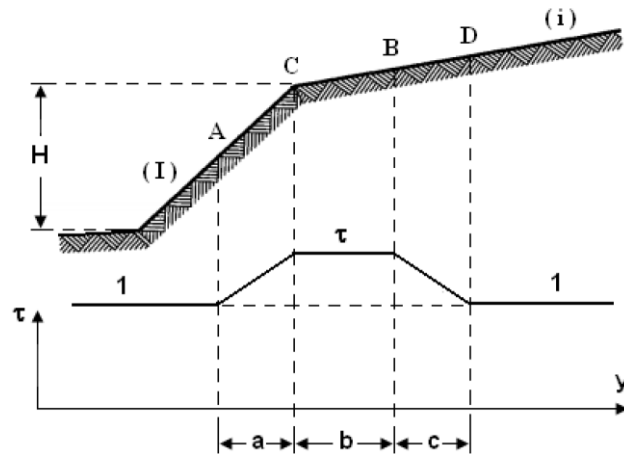
- $S_T$  should be applied for slopes that belong to a 2D-topographic irregularity greater than about 30 meters. It is not stated specifically whether this implies height or projected height.
- $S_T$  should be applied for slopes steeper than about  $15^\circ$ .
- $S_T \geq 1.2$  near the top edge of isolated slopes, or embankments with slope angles lower than  $30^\circ$ .
- $S_T \geq 1.4$  near the top edge of embankments with slope angles greater than  $30^\circ$ .
- In the presence of a loose surface layer (undefined) above values should be increased by at least 20%.
- The value of  $S_T$  may be assumed to decrease as a linear function of the height above the base, and to be unity at the base. Hereto it is added that for failure surfaces near the base, in pseudo-static analyses topographic effects may be neglected.

Gallipoli et al. (2013) give a visual impression of the Italian seismic code NTC08 and this seems to be in full agreement with the above EN1998-5 provision. They interpret the aforementioned 30 meters of the topographical irregularity as being 30 meters in vertical direction.

The provision on topographic amplification in the French code PS-92 was obtained indirectly from the doctoral thesis by Nguyen (2015) (in French). Nguyen et al. (2013) note that this code was applicable until October 31<sup>st</sup> 2012 after which above provision from EN 1998-5 became obligatory [ref. 3, ref. 12]. The magnitude and horizontal extent of the amplification factor  $\tau$  is presented in figure 2.6. Herein:

- $\tau$  is the amplification factor.
- $I$  is the tangent of the slope with height  $H$ .
- $i$  is the tangent of the soil behind the crest.
- $a$ ,  $b$  and  $c$  give the horizontal extent over which the seismic amplification should be accounted for.

Figure 2.6 Variation of the cross-sectional amplification factor according to the French code PS-92 (1995) [ref. 15]



Herein:

- $\tau = 1$  for  $I - i < 0.4$ ;
- $\tau = 1 + 0.8(I - i - 0.4)$  for  $0.4 \leq I - i \leq 0.9$ ;
- $\tau = 1.4$  for  $I - i > 0.9$
- $a = H/3$   $b = \min\{20I ; (H + 10)/4\}$   $c = H/4$

Above provision can be applied if the following conditions are met:  $H \geq 10$  meters and  $i \leq 1/3$ .

The Seismic Design Guidelines for Dikes (2014) in British Columbia (Canada) adopt a topographic modification factor  $Ampl_{apex}$  which too is independent of site amplification. No applicability range is provided and the amplification factor is applied only to the peak ground acceleration at the crest of the dike. For the magnitude of the modification factor reference is made to Faccioli (1991) who provides an

approximation to an exact solution of SH-waves approaching a wedge. As suggested by the example provided in Appendix F, this comes down to determining the ratio between  $180^\circ$  and the apex angle of the crest. In terms of the slope  $I$  from figure 2.6 this implies:

$$Ampl_{apex} = \frac{180^\circ}{180^\circ - \text{atan}(I)}$$

No minimum height of the slope is mentioned at which the modification factor should be applied. Moreover, the factor is used in defining the PGA level that is used for both the liquefaction analysis and the pseudo-static stability analysis, implying that the amplification is not merely a superficial effect.

## 2.3 Synthesis

The findings from e.g. Ashford et al. (1997) and Bouckovalas & Papadimitriou (2006) and the implementation of  $S_T$  from appendix A of EN 1998-5, seem to suggest that stratigraphic and topographic amplification effects can be addressed independently. More recently, different authors (Tripe et al. (2013), Rizzitano et al. (2014)) suggest that the two effects are in fact not independent and that from a fundamental perspective the effects should be accounted for simultaneously in a non-linear dynamic analysis. However, from a practical perspective this will not be feasible in all cases.

Witteveen+Bos in an earlier study [ref. 6] performed a sensitivity analysis into the effects of topographic amplification at artificial dwelling hills, by performing dynamic non-linear time history analyses in PLAXIS-2D. Herein site geometries, subsoil stratification and acceleration time histories were varied. The results hereof were presented in terms of peak ground velocities as this is a metric relevant for building damage and can be compared with SBR guidelines [ref. 18].

In the present study we will consider peak ground accelerations for two reasons:

- The question in the Request for Offer was raised specifically towards peak ground accelerations.
- Reference values from literature are predominantly about accelerations which allows for comparison.

In the present study calculations from this sensitivity analysis have been updated using more recently available recorded signals at 5 downhole G-station arrays (depth 50 meters) in two directions: East-West and North-South. It is noted that the recorded signals carry the name of the location at which the signals are recorded. In the present study this location is not relevant as a sensitivity analysis is performed in which all recorded signals are applied to all characteristic sites A, B, C and D. These sites refer to four different stratigraphic profiles of which the average shear wave velocity in the upper 10 meters  $V_{s10}$  [m/s] is provided in table 2.2. For more detail on these profiles one is referred to [ref. 6].

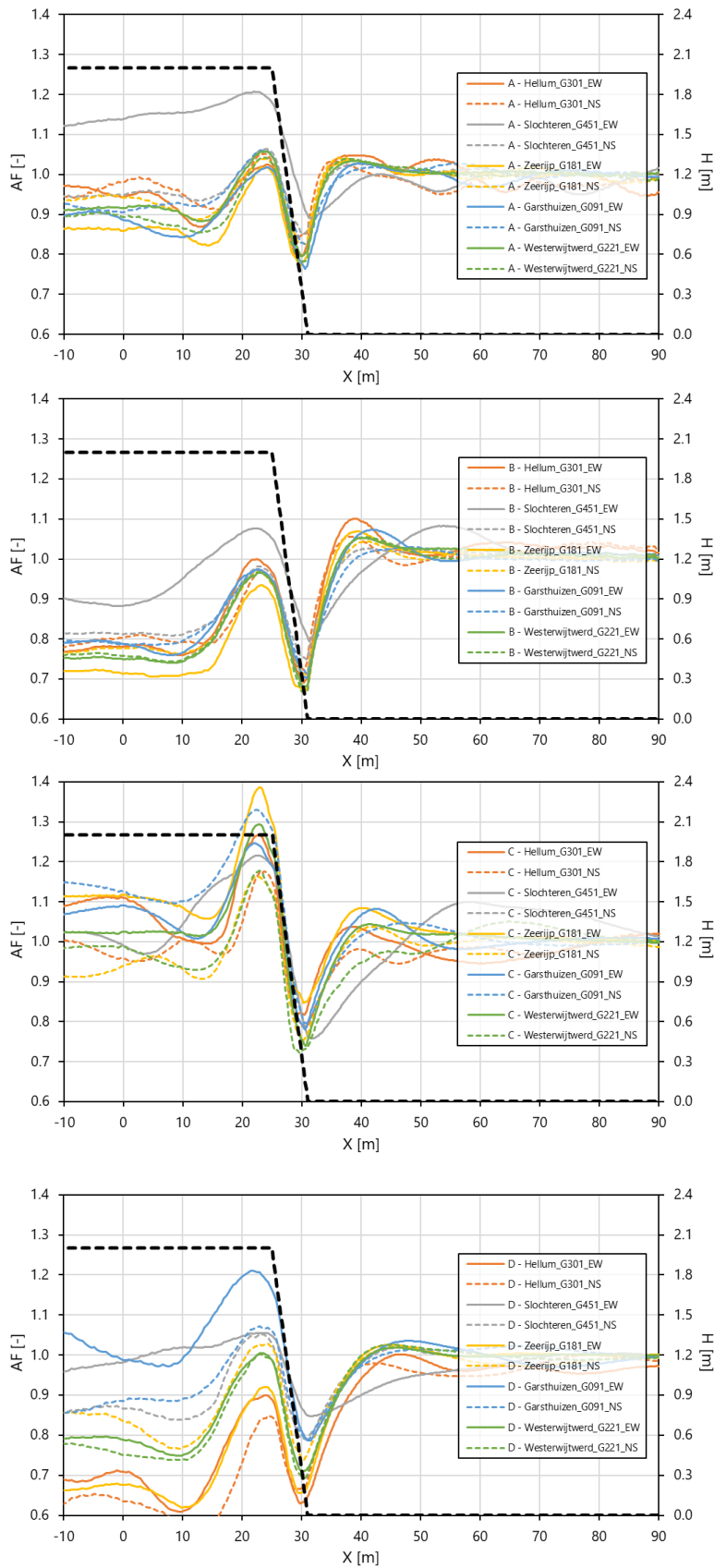
The output from these calculations is presented in figure 2.7 in terms of amplification factors (AF) of the maximum horizontal acceleration during dynamic loading  $a_{x,max}(x)$  divided by the maximum horizontal acceleration calculated for free field conditions  $a_{x,max}(ff)$ .

In figure 2.7 it is observed that at sites A and B, the Slochteren\_G451\_EW signal is dominant compared to the other signals with regard to calculated maximum amplification. At site C, the Zeerijp\_G181\_EW signal is dominant and the maximum amplification of all acceleration time histories at the crest exceeds 1.0. At site D, the Garsthuizen\_G091\_EW signal is dominant, but the variety in (de-)amplification between the signals is significant.

Based on these findings the following can be stated:

- Only geometrical properties are insufficient to describe correctly the topographic amplification.
- A particular signal does not provide a large amplification at all sites, nor does one sites provide merely high amplification factors for all signals. This underlines the conclusion by Tripe et al. (2013) that natural site- and topographic amplification cannot be treated separately.
- Topographic amplification is a relevant phenomenon at slopes with heights significantly lower than suggested by various international code provisions.

Figure 2.7 Calculated amplification factors AF near a 2 meter high 1:3 slope for 10 acceleration time histories. From top to bottom the results for sites A, B, C and D are presented. The black dashed line represents the site geometry of which the height H is presented on the secondary vertical axis.



Given these observations the obvious question becomes: ‘what would be a suitable method to account for topographic amplification?’. Based on findings from recent numerical studies, it may from a physical perspective be preferable to perform analyses in which the stratigraphic and topographic amplification effects are combined. However, from an engineering- and code-making perspective it is understandable that both effects are treated independently. The most detailed, yet relatively easy to apply methods are given by Bouckovalas & Papadimitriou (2005) and Nguyen (2015). Since the exact details of the latter are in French and therefore not well understood, the former will be compared with the results presented in figure 2.7.

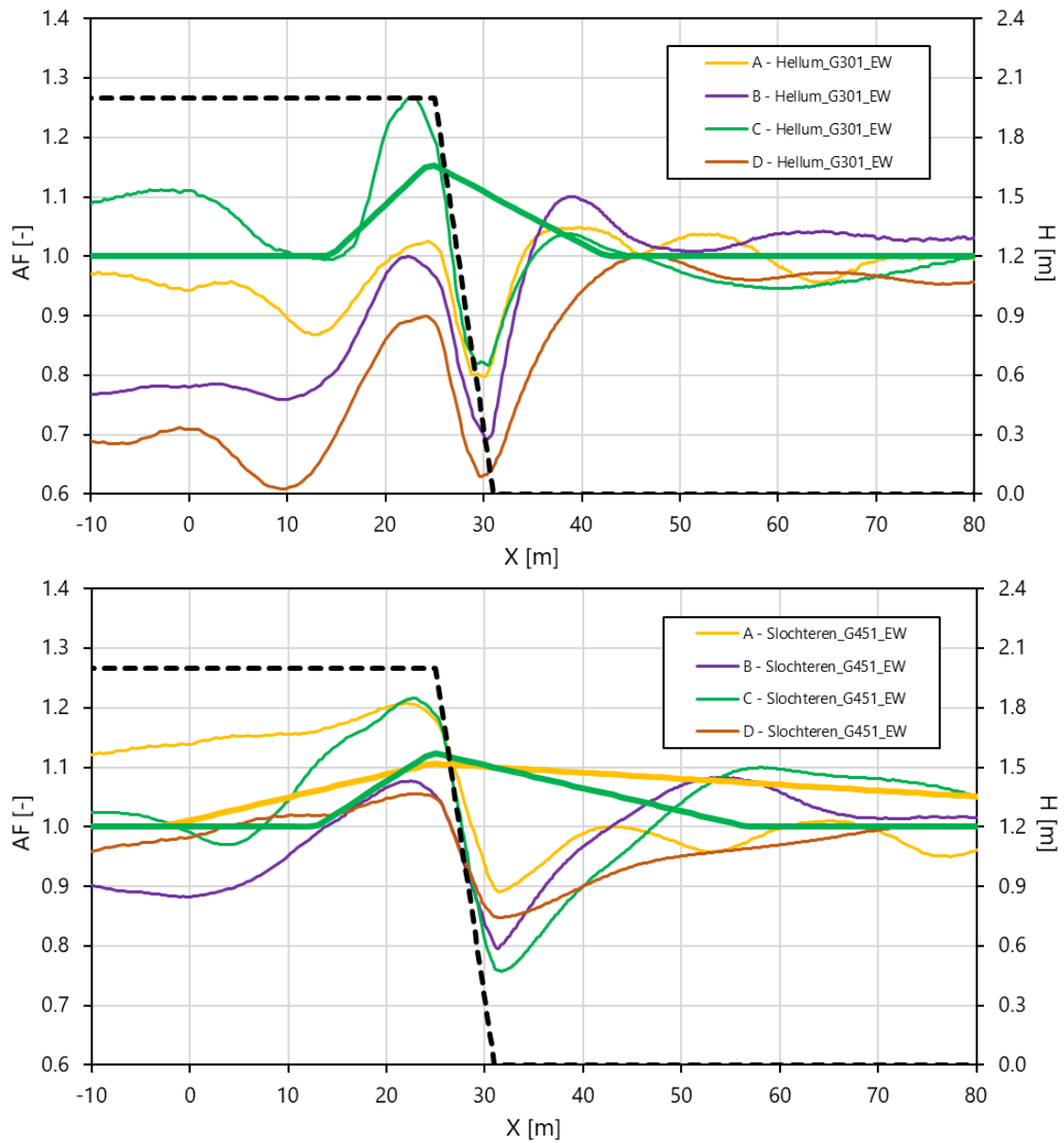
This comparison is made in table 2.2 and figure 2.8. To apply the method by Bouckovalas & Papadimitriou (2015), the predominant wavelength of input motion  $\lambda$  is obtained from the recorded signals. For the shear wave velocity, the averaged shear wave velocity in the upper 10 meters  $V_{s10}$  is used.

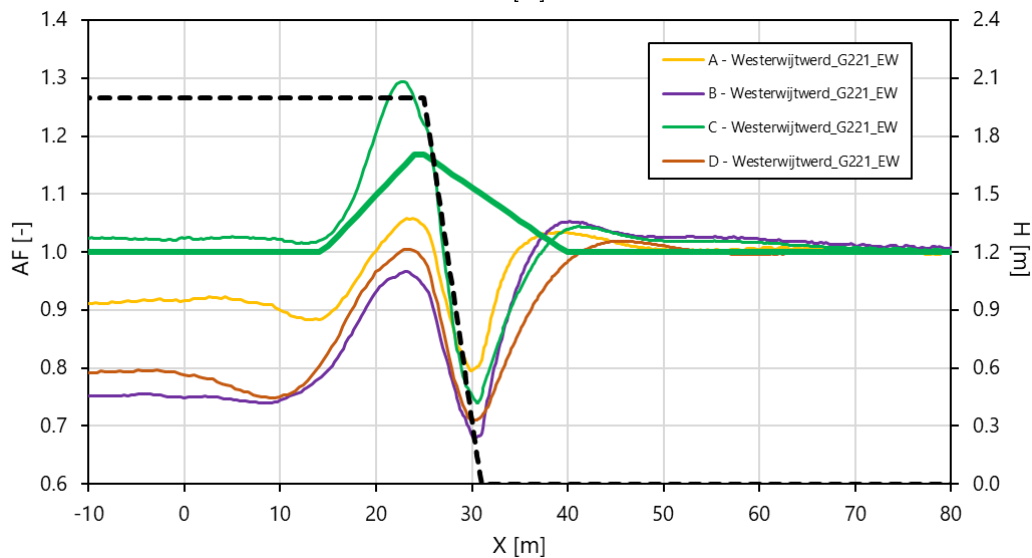
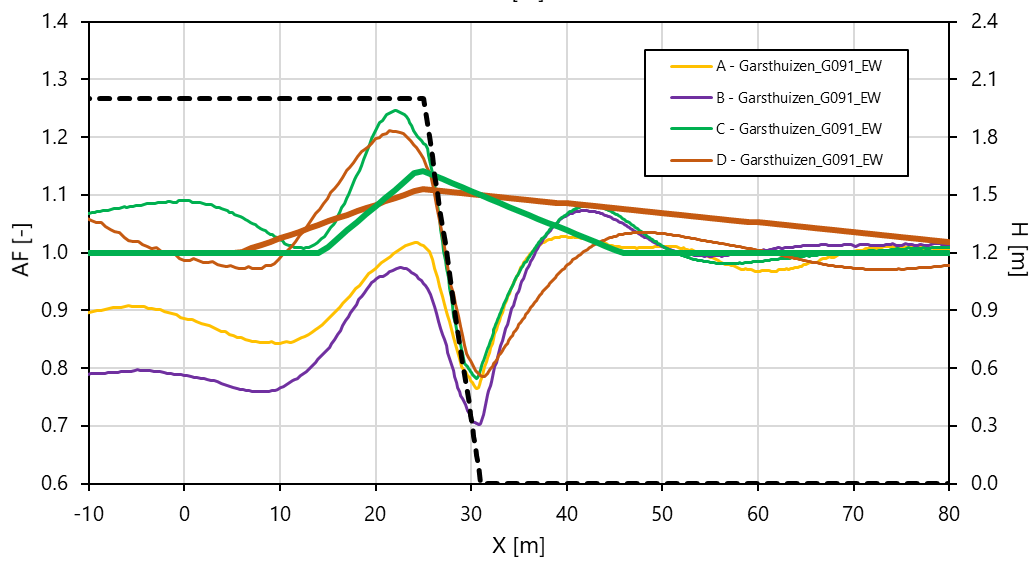
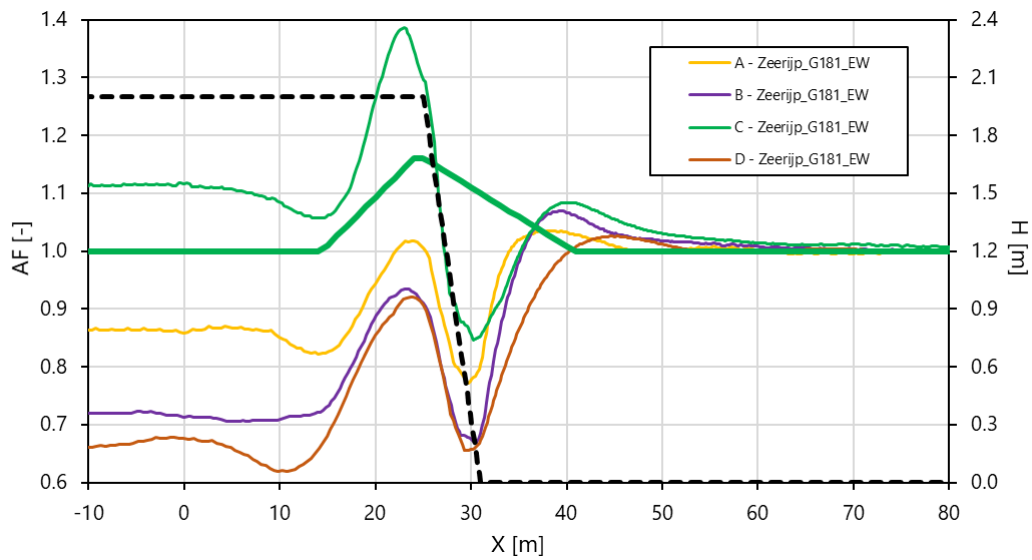
table 2.2 shows for each recorded signal, the maximum amplification factor that is calculated in the present study using PLAXIS-2D (*calc*) and the value obtained using the method by Bouckovalas & Papadimitriou (2015) (*BP*). In figure 2.8 for 5 EW records the maximum calculated amplification factors are presented for the sites A, B, C and D. For the highest calculated amplification factor(s) per record, the proposed amplification factor envelope(s) by Bouckovalas & Papadimitriou (2005) are given in the same plot.

Table 2.2 Predominant frequencies of recorded input motions, averaged shear wave velocities of the upper 10 meters per site and calculated (*calc*) versus predicted amplification factors using the method from Bouckovalas & Papadimitriou (2005) (*BP*)

record	station	dir	pred. freq.	site A		site B		site C		site D	
				<i>calc</i>	<i>BP</i>	<i>calc</i>	<i>BP</i>	<i>calc</i>	<i>BP</i>	<i>calc</i>	<i>BP</i>
Hellum	G301	EW	10.7 Hz	1.03	1.13	1.00	1.14	1.27	1.15	0.90	1.12
Hellum	G301	NS	10.6 Hz	1.05	1.13	0.97	1.14	1.18	1.15	0.85	1.12
Slochteren	G451	EW	6.3 Hz	1.21	1.11	1.08	1.12	1.22	1.12	1.06	1.10
Slochteren	G451	NS	11.3 Hz	1.06	1.13	0.98	1.15	1.21	1.16	1.05	1.12
Zeerijp	G181	EW	12.3 Hz	1.02	1.14	0.93	1.15	1.39	1.16	0.92	1.13
Zeerijp	G181	NS	3.9 Hz	1.04	1.09	0.97	1.10	1.16	1.10	1.03	1.08
Garsthuizen	G091	EW	8.8 Hz	1.02	1.12	0.97	1.13	1.25	1.14	1.21	1.11
Garsthuizen	G091	NS	8.8 Hz	1.06	1.12	0.97	1.13	1.33	1.14	1.07	1.11
Westerwijtwerd	G221	EW	13.5 Hz	1.06	1.14	0.97	1.16	1.29	1.17	1.01	1.13
Westerwijtwerd	G221	NS	13.7 Hz	1.04	1.14	0.97	1.16	1.18	1.17	1.00	1.13

Figure 2.8 Calculated amplification factors AF near a 2 meter high 1:3 slope at sites A, B, C and D. From top to bottom the signals Hellum\_G301\_EW, Slochteren\_G451\_EW, Zeerijp\_181\_EW, Garsthuizen\_G091\_EW & Westerwijtwerd\_G221\_EW. The fat coloured lines represent the amplification factor envelope(s) as proposed by Bouckovalas & Papadimitriou (2005), corresponding (in equal colour) to the highest calculated amplification factor(s) per signal. The black dashed line represents the site geometry of which the height H is presented on the secondary vertical axis





With respect to the results presented table 2.2 and figure 2.8, the following remarks are made:

- For the calculated values (*calc*) of the amplification factor presented in table 2.2, only the 'sloped' zone is considered (thus where  $0 < X < 31$  with reference to the horizontal axes in figure 2.7 and figure 2.8).

- In the procedure from Bouckovalas & Papadimitriou (2015) the amplification increases with decreasing  $V_s$  which is in agreement with the observations that the highest calculated amplification is found at site C. However, site B has a relatively low shear wave velocity characteristic in the upper 10 meters too and yet the calculated amplification factors are comparably low as the much stiffer site D. It has not been investigated in further detail what causes this discrepancy. The only notable difference between site B and the other sites is that the stratigraphic impedance of the soil profile is lower;  $V_s < 180 \text{ m/s}$  up to a depth of approximately 30 meters. Related to this, the choice of the 10 meters depth over which the shear wave velocity is averaged is arbitrary and mostly driven by how the subsoil is modelled in [ref. 6].
- The dependency between stratigraphic and topographic effects is once more exemplified, as the amplification factors from the Slochteren\_G451\_EW signal at site A and from the Garsthuizen\_G091\_EW signal at site D reach values of 1.2, whereas the amplification of the same signals at other sites is far less pronounced.
- Qualitatively the horizontal extent at which amplification is calculated, is captured reasonably well by the procedure by Bouckovalas & Papadimitriou (2015).
- Disregarding the 30 meter height criterium, using the provision from EN 1998-5 leads to a topographic amplification factor  $S_T$  of 1.2, given that the slope is 1:3 (= 18.4°).

The depth effect in terms of velocities and accelerations in EN 1998-5 is assumed to be linear towards the base according to clause A.2(d). However, in clause A.3 it is stated that seismic amplification decreases rapidly with increasing depth. Therefore the effect may be neglected in pseudo-static analyses in which the failure surface passes near the base. This is in line with recent study results by Witteveen+Bos (other than the present study discussed in this paragraph) in which the amplification is shown to be very superficial in dynamic non-linear finite element analyses involving revetment slopes.

## 2.4 Conclusions and recommendations

- As noted at the very beginning of this chapter, the effect of topographic irregularities on ground motion are by definition not captured by performing 1D-site response analyses and are therefore not included in the site response model of the present GMM.
- Based on the literature overview from section 2.2, it is concluded that topographic and stratigraphic amplification cannot be assessed independently and therefore from a fundamental perspective both aspects should be considered simultaneously. This requires significant computational effort.
- From a code perspective it is preferable to have a simple approach and therefore to treat topographic and stratigraphic amplification independently. This is the currently implemented in Eurocode 8. Stratigraphic amplification is determined in EN1998-1 by the Ground type that defines the soil factor  $S$  and thereby the coordinates of the elastic design response spectrum. By including topographic amplification as per EN1998-5 these ordinates ( $y$ -values) are multiplied with the topographic factor  $S_T$ .
- Considering the above there are two issues:
  - Based on the results presented in section 2.3 significant topographic amplification (up to 40 % compared to free field conditions) can occur at slope heights disregarded by EN1998-5.
  - There currently does not appear to a method that adequately captures the physical complexity of the phenomenon, but yet is easy to apply.
- The proposed method by Bouckovalas & Papadimitriou (2005), although explicitly being indicative, up front appears to give a reasonable balance between simplicity and accuracy. By comparison with calculation results in the present study, it is observed that the spatial extent over which amplification plays a role is predicted rather well. The largest amplification factors calculated in the present study are higher than what the method by Bouckovalas & Papadimitriou (2005) predicts. In many cases however the calculations provide values that are lower than the proposed minimum value of 1.1.
- As it is observed that topographic amplification can occur at relatively low slope heights, taking some factor into account seems appropriate. Advantage of the method proposed by Bouckovalas & Papadimitriou (2006) and the French code PS-92 is that the spatial extent over which amplification plays a role is mentioned explicitly. The latter can be applied if for application the slope height criterium of  $H \geq 10$  is dismissed. Currently there is too little numerical simulation data to substantiate the preference of a certain method.

- As noted in section 2.3, in this study the amplification of the (horizontal) peak ground acceleration is assessed. Results for higher spectral periods have not been extracted and analysed, but it is very well possible to do so. Although the considered soil profile A to D in [ref. 6] are selected to represent various typical Groningen soil conditions, the number of considered subsoil profiles (and slope geometries) is too limited to draw region-wide conclusions in terms of outcome envelopes. If a study is conducted towards the amplification at higher spectral accelerations, it is therefore recommended to include more soil profiles and geometric variability.

## 2.5 References

- 1 Ashford, S.A., Sitar, N. 1997. Analysis of Topographic Amplification of Inclined Shear Waves in a Steep Coastal Bluff. *Bulletin of the Seismological Society of America*. Vol. 87, No. 3, pp. 692-700.
- 2 Ashford, S.A., Sitar, N., Lysmer, J., Deng, N. 1997. Topographic Effects on the Seismic Response of Steep Slopes. *Bulletin of the Seismological Society of America*. Vol. 87, No. 3, pp. 701-709.
- 3 Athanasopoulou, A., Dimova, S., Fuchs, M., Sousa, M.L., Pinto, A., Nikolova, B., Iannaccone, S. 2018. State of Eurocode 8 implementation in the European Union. *Proceedings of the 16<sup>th</sup> European Conference on Earthquake Engineering*, Thessaloniki.
- 4 Bouckovalas, G.D., Papadimitriou, A.G. 2005. Numerical evaluation of slope topography effects on seismic ground motion. *Soil Dynamics and Earthquake Engineering* 25, pp. 547-558.
- 5 Bouckovalas, G., Papadimitriou, A. 2006. Aggravation of seismic ground motion due to slope topography. *First European Conference on Earthquake Engineering and Seismology*. Paper number: 1171.
- 6 Bouzoni, E., Besseling, F., Slob, S. 2018. Local effects of artificial dwelling hills and canals on ground response during induced earthquakes. *Proceedings of the 16<sup>th</sup> European Conference on Earthquake Engineering*, Thessaloniki.
- 7 CEN. 2004. EN 1998-1 - Eurocode 8: Design of structures for earthquake resistance - Part 1: General rules, seismic actions and rules for buildings.
- 8 CEN. 2004. EN 1998-5 - Eurocode 8: Design of structures for earthquake resistance - Part 5: Foundations, retaining structures and geotechnical aspects.
- 9 Faccioli, E. (1991). Seismic Amplification in the Presence of Geological and Topographic Irregularities. *Proceedings of the Second International Conference on Recent Advances in Geotechnical Earthquake Engineering and Soil Dynamics*, St. Louis, Missouri, USA, Paper no. SOA7.
- 10 Geli, L., Bard, P., Jullien, B. 1988. The effect of topography on earthquake ground motions: a review and new results. *Bulletin of the Seismological Society of America*, Vol. 78, No. 1, pp. 42-63.
- 11 Golder Associates, 2014. *Seismic Design Guidelines for Dikes 2<sup>nd</sup> Edition*. Ministry of Forests, Lands and Natural Resource Operations.
- 12 Martin, F. de. 2013. Effets topographiques 2D en sismologie - Vérification des coefficients simplifiés Eurocode 8 par éléments spectraux. <https://hal-brgm.archives-ouvertes.fr/hal-00785027>.
- 13 NEN. 2018. NPR9998 - Assessment of structural safety of buildings in case of erection, reconstruction and disapproval - Induced earthquakes - Basis of design, actions and resistances (in Dutch).
- 14 Nguyen, H.T., Fleurisson, J., Cojean, R. 2013. Evaluation of topography site effect in slope stability under dynamic loading. *Vienna Congress on Recent Advances in Earthquake Engineering and Structural Dynamics*, Vienna, Austria, Paper no. 521.
- 15 Nguyen, H.T. 2015. Évaluation des effets de site topographiques dans les pentes soumises à des sollicitations dynamiques par simulations numériques. *Géologie appliquée. Ecole Nationale Supérieure des Mines de Paris* (French).
- 16 Nuove Norme Tecniche per le Costruzioni, 2008. [http://www.geologi.it/leggi/dm-14-01-2008\\_cap-03.pdf](http://www.geologi.it/leggi/dm-14-01-2008_cap-03.pdf) (Italian, accessed on 12 March, 2019).
- 17 Rizzitano, S., Cascone, E., Biondi, G. 2014. Coupling of topographic and stratigraphic effects on seismic response of slopes through 2D-linear and equivalent linear analyses. *Soil Dynamics and Earthquake Engineering* 67, pp. 66-84.
- 18 SBRCURnet. 2017. *SBR Trillingsrichtlijn A: Schade aan bouwwerken: 2017*. Delft. The Netherlands.
- 19 Tripe, R., Kontoe, S., Wong, T.K.C. 2013. Slope topography effects on ground motions in the presence of deep soil layers. *Soil Dynamics and Earthquake Engineering* 50, pp. 72-84.

- 20 Zhang, Z., Fleurisson, J., Pellet, F. 2018. The effects of slope topography on acceleration amplification and interaction between slope topography and seismic input motion. *Soil Dynamics and Earthquake Engineering* 113, pp. 420-431.

# 3

## LATERAL SPREADING

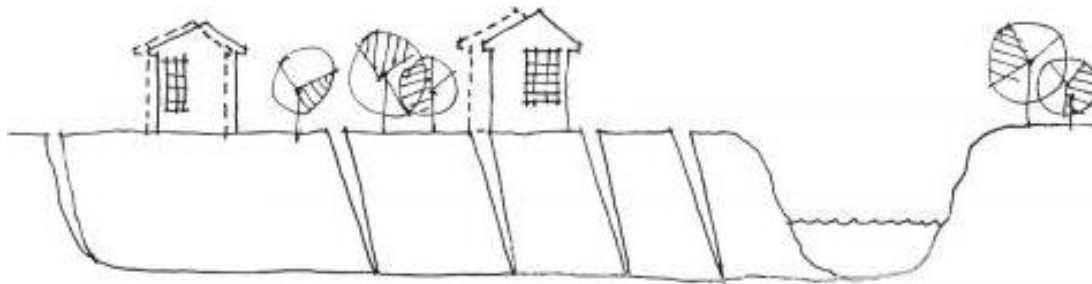
### 3.1 Description of the phenomenon

Kramer (2013) provides the following definition of lateral spreading: *Lateral spreading is the finite, lateral movement of gently to steeply sloping, saturated soil deposits caused by earthquake-induced liquefaction.* The consequences of lateral spreading are potentially devastating as the surface may displace horizontally for several meters, causing significant damage to infrastructure and housing.

It is important to emphasize that the precondition for lateral spreading to occur, is earthquake-induced liquefaction. Several definitions of liquefaction exist, but in general it is described as the state in which a saturated granular material has negligible stiffness and strength, comparable to a thick fluid. This state can be reached by repetitive shearing of the granular material during an earthquake in which loosely packed granular materials are most susceptible due to their contractive nature under shearing.

In the present study we will not consider the likelihood of a soil in Groningen liquefying. For the assessment of liquefaction potential we use the Groningen-specific assessment procedure developed by Green et al. (2018) that is also incorporated in the NPR 9998 [ref. 24]. An indicative overview of the presence of loosely packed sands in the shallow Groningen subsurface can be found in [ref. 18], findings and discussion on what earthquake magnitude is needed to induce liquefaction can be found in [ref. 12] and findings on the likelihood of surficial liquefaction manifestations in Groningen can be found in [ref. 11].

Figure 3.1 Schematic representation of the phenomenon lateral spreading [ref. 6]



In the remainder of this chapter the above definition of lateral spreading from Kramer (2013) will be used. Adhering to the Request for Offer the focus will be on lateral spreading at free faces, as visualized by the schematic representation of figure 3.1. It is noted that the term 'free face' will be used in the remainder of this chapter, rather than 'slope', 'levee' or 'river bank'. Bartlett & Youd (1995) explain the term as an 'abrupt topographical depression' but no definition of the steepness is provided in literature. As discussed later in this chapter, in the prediction models lateral spread displacements are a function of distance from the free face toe, rather than its steepness.

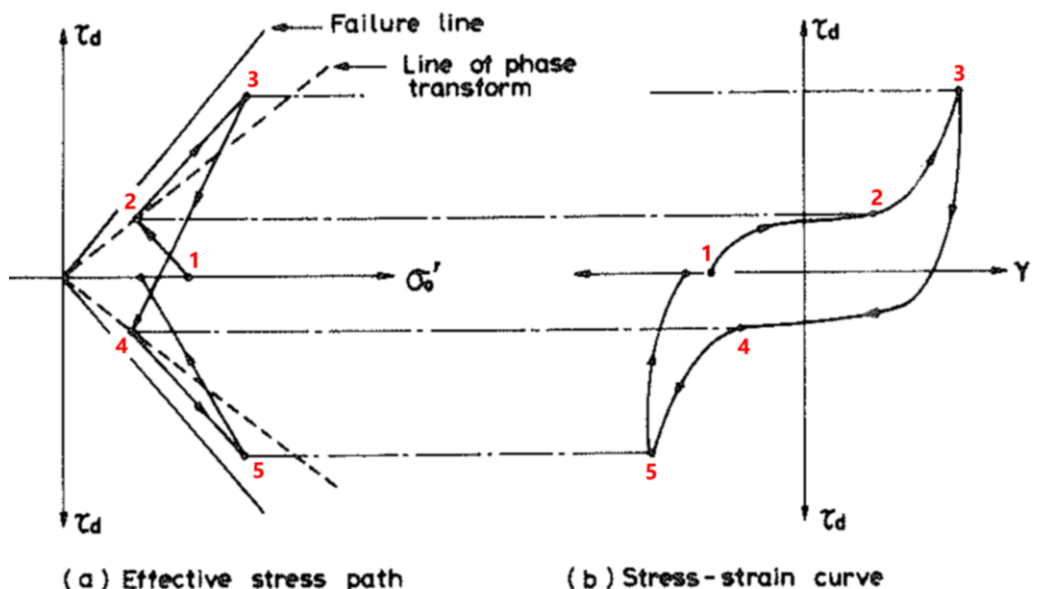
By using this definition and focus the knowledge gap is filled between the following stability issues that will explained below:

- Inertial instability displacements without shear strength reduction. These are expected to be small and more importantly have a limited horizontal extent. Associated displacements can be quantified by performing Newmark- or non-linear dynamic finite element analyses.
- Flow failure displacements. These are difficult to quantify accurately, but the mechanism can be identified by assessing the (macro-) stability near free faces using the post-liquefaction residual strength. This check can be performed using relatively simple limit equilibrium stability software.

Youd (1973) from a fundamental perspective summarizes some of the characteristics of the phenomenon of lateral spreading by referring to the behaviour observed in static- and cyclic laboratory tests:

- Lateral spreading deformation is the summation of repeated steps of limited flow. Limited flow occurs if during cyclic loading shear stress reversals occur, causing a repeating pattern of contraction followed by dilative solidification. The effective stress ( $\sigma'_v$ ) and stress-strain ( $\tau_d - \gamma$ ) behaviour of one cycle is shown in figure 3.2 indicated by arrows. Movement towards the line of phase transformation indicates contraction (large strains upon increase of shear stress, paths 1-2 and 3-4) after which dilative solidification occurs (smaller additional strains upon further increase of shear stress, paths 2-3 and 4-5).
- Lateral spreading is typically expected to occur at gently sloping ground surface conditions.
- If slopes are too steep, no stress reversal occurs because the static shear stresses are too high. For dense soils this tends to increase the liquefaction resistance (Vaid & Chern, 1983), for loose soils this at some point in time results in unlimited flow, which only stops when the driving shear forces are reduced to values below the viscous resistance of the flowing material.
- If slopes are too gentle, there is no gradient to cause a preferential horizontal direction in which the soil body displaces.
- At restabilization during a stress reversal loosening of the material may occur, caused by a combination of dilation of the material (creating voids) and the availability of excess water to fill these voids. Even after reconsolidation the soil may be left in a state that is comparable or looser than the initial condition.
- Limited flow deformation can occur only as long as ground shaking occurs and displacements would restabilize and thereby stop immediately after shaking.

Figure 3.2 Illustration of cyclic mobility behaviour of dense sand [ref. 17]



With respect to analysis procedures for the mechanisms above, Kramer (1996) provides distinction between inertial instability and weakening instability problems:

- Inertial instability occurs when inertia forces during the earthquake cause temporal instability, but the shear strength remains unaffected, thus resulting in, although displaced, equilibrium after the

earthquake. For an estimation of the displacement a Newmark approach can be applied, if needed substantiated by performing non-linear dynamic finite element analyses.

- Weakening instability in which the shear strength of the soil is reduced by effects of liquefaction:
  - If in this case static equilibrium is not found, flow failure can be expected to occur. This will result in fluid-like behaviour and displacements that are in general far beyond the calculation capability of common geotechnical software. Such cases have been back-analysed to obtain post-liquefaction shear strengths (Olson & Stark, 2002) which can be applied as a minimum value of the residual liquefied strength.
  - If static equilibrium is found, deformation failure can occur, but the post-earthquake situation is stable and the displacement thus ceases after shaking. Depending on the intensity and duration of shaking, significant displacements up to several meters have been observed during/after tectonic earthquakes worldwide. This is in fact lateral spreading and this chapter will consider simplified analysis procedures to predict this displacement.

Due to topographic- and soil heterogeneity in practice often a combination of lateral spreading and flow failure (or slumping) mechanisms is observed. Cubrinovski et al. (2012) make a distinction between a 'block-mode' failure and an 'exponential-decay' ground deformation pattern near Kaiapoi, New Zealand, following the 2010 Darfield earthquake. The former shows the horizontal movement of a near intact soil body, the latter shows large horizontal deformations near the waterway which exponentially decreases at increasing distance from the river bank. Close to the river bank it is likely that multiple mechanisms play a role simultaneously. As Zhang et al. (2004) note the mechanisms of lateral spreading and local slumping failure are fundamentally different, they have removed all instances in which the distance from the free face is smaller than four times the free face height from their lateral spreading case history database.

In the Request for Offer reference is made to lateral spreading along the Meuse levees as a result of the Roermond earthquake in 1992. At a specific location opposite of Buggenum indeed finite horizontal deformations in excess of a meter have been observed, caused by liquefaction of which visual evidence was observed nearby [ref. 27]. Photographs also show near vertical offsets in the post-earthquake ground surface, indicating rotational slope failure rather than lateral spreads. As indicated above, in reality likely a combination of several mechanisms has occurred.

### 3.2 Literature overview

As the consequences of lateral spreads can be so devastating, numerous publications on the subject can be found, varying from centrifuge tests to advanced numerical modelling. The aim of this paragraph is not to give a complete overview of all research from the past decades, but to give a fair idea of what methods are currently available to estimate the magnitude of lateral spreading and discuss their (dis-) advantages.

Hamada et al. (1987) set-up the following empirical relation to determine the liquefaction-induced horizontal ground displacement  $D_H$ , based on ground displacement vectors (e.g. figure 3.4) during the 1964 Niigata and 1983 Nihonkai-Chubu earthquakes in Japan.

$$D_H = 0.75 \sqrt[2]{H_{liq}} \sqrt[3]{S}$$

Herein:

$H_{liq}$  is thickness of the liquefied soil layer in m

$S$  the higher of the surface slope and the gradient of the bottom of the liquefied layer in %

Hamada (1999) extends this relation by including of acceleration time history and a measure of soil strength. The proposed relation below is calibrated using model tests and validated by comparison with 10 site observations during 3 earthquakes in Japan, including two observations during the 1995 Kobe earthquake.

$$D_H = \frac{0.0125 \cdot \sqrt{H_{liq}} \cdot S}{\bar{N}^{0.88}} \cdot \sum_i^n A_i^{0.48} T_i$$

Herein:

$\bar{N}$  is the normalized Standard Penetration Test (SPT) value [-], being approximately equal to  $(N_1)_{60}$   
 $A_i$  is the maximum horizontal acceleration of segment  $n$  of the acceleration time history in gal (= 0.01 m/s<sup>2</sup>)  
 $T_i$  is the duration of the same segment  $n$  of the acceleration time history in seconds

Bartlett & Youd (1992, 1995) performed a statistical analysis on observed lateral spreading sites observed after 8 major earthquakes in Japan and the United States reported in several NCEER reports. Using a multi-linear regression analysis two empirical models are set up that can be used to predict the displacement; one for gently sloping ground conditions and one for free face conditions. Youd et al. (2002) revised this empirical model by implementing some updates on the functional form of the prediction equation, the reassessment of same data and the addition of data from three other earthquakes. The resulting prediction equations are often referred to (e.g. O'Rourke & Liu (2012)) and for free face conditions it reads:

$$\log(D_H) = -16.713 + 1.532 M - 1.406 \log R^* - 0.012 R + 0.592 \log W + 0.540 \log T_{15} + 3.413 \log(100 - F_{15}) - 0.795 \log(D50_{15} + 0.1)$$

Herein:

$M$  is the earthquake moment magnitude [-]

$R$  is the nearest horizontal site-to-source distance in km

$R^*$  is an adjusted distance parameter as a function of  $M$  and  $R$

$W$  is the free face ratio  $H/L$  expressed as a percentage. Herein  $H$  is the free face height in m and  $L$  the horizontal inland distance from the free face base (= toe of the slope)

$T_{15}$  is the cumulative thickness in meters of saturated granular layers with a corrected SPT blow count  $(N_1)_{60}$  lower than 15, which using the equivalence relation adopted by Idriss & Boulanger (2008) corresponds to a relative density  $D_R$  of 57 %. The relative density is a measure of the state between the loosest possible granular configuration (0%) and densest possible granular configuration.

$F_{15}$  is the average fines content in % for the granular materials within  $T_{15}$

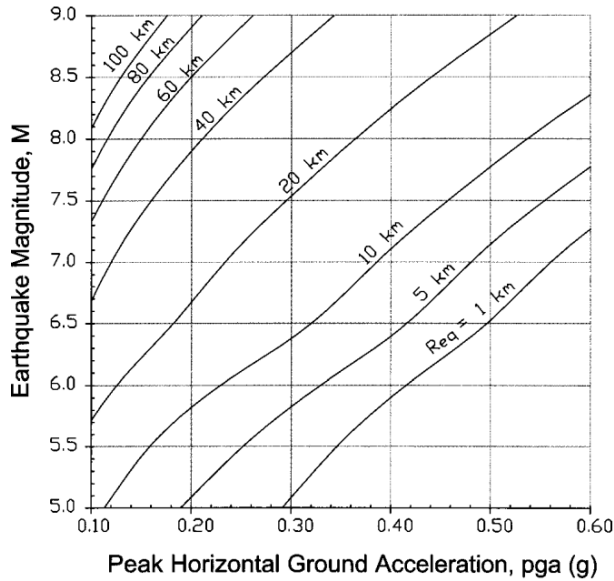
$D50_{15}$  is the average mean grain size in mm for the granular materials within  $T_{15}$

The prediction equation for sloping ground conditions uses largely the same parameters and reads:

$$\log(D_H) = -16.213 + 1.532 M - 1.406 \log R^* - 0.012 R + 0.338 \log S + 0.540 \log T_{15} + 3.413 \log(100 - F_{15}) - 0.795 \log(D50_{15} + 0.1)$$

Important assumption in deriving above two relations by Youd et al. (2002) is the implicit attenuation relation that limits applicability to stiff sites in Japan and the western part of the United States. For soft soil sites at which significant amplification is expected, an equivalent distance term  $R_{eq}$  can be obtained from figure 3.5 which represents an average from three different attenuation relations.

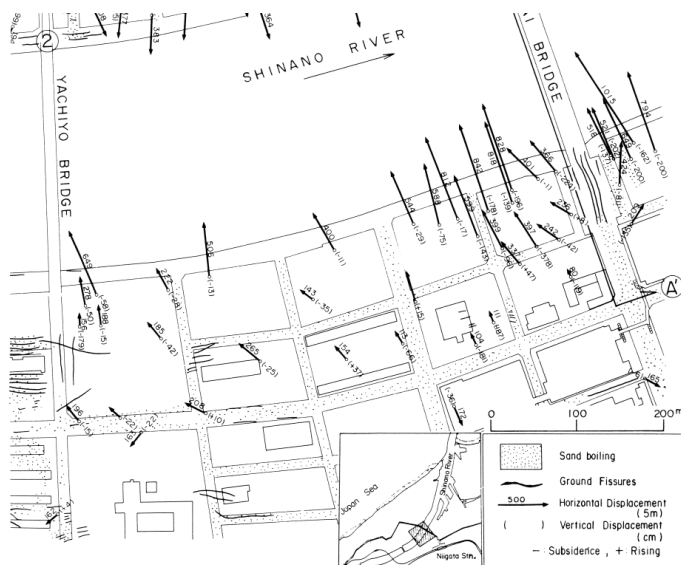
Figure 3.3 Graph for determining equivalent source distance  $R_{eq}$  [ref. 30]



Zhang & Zhao (2005) note that the database of magnitudes and source distances underlying the method by Youd et al. (2002) is poorly distributed and moreover that different faulting mechanisms may have an effect. They moreover note that the database is dominated by the Niigata 1964 earthquake as most displacement vectors were measured at that event. The number of displacement vectors does however not coincide with the number of independent events (see figure 3.4).

Franke & Stewart (2014) incorporate the method by Youd et al. (2002) in a probabilistic framework to be able to combine all possible earthquake scenarios and their weighted likelihood. Hereby the robustness to the large sensitivity of varieties in  $M$  and  $R$  is increased, albeit at the cost of computational effort. They moreover note that the standard deviation on a log-scale from the Youd et al. (2002) procedure is 0.197 on log scale which in terms of predicted settlement implies coefficient of variation of 0.57.

Figure 3.4 Permanent ground displacements in the upstream area of the Shinano River after the 1964 Niigata earthquake [ref. 14]

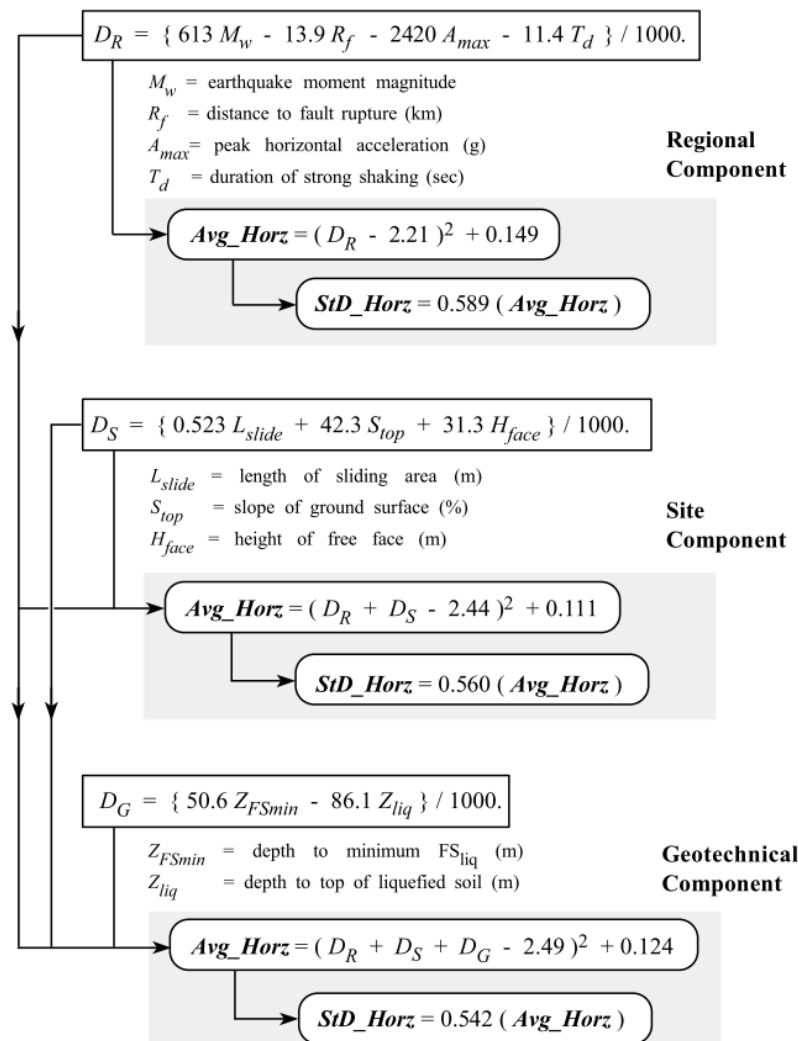


Where Youd et al. (2002) base their prediction on the assessment of individual displacement vectors as shown in figure 3.4, Rauch (1997) comprised a large database of in total 78 independent lateral spreading events (or slide areas), observed during 16 earthquakes over the period 1906 - 1994. Per location as much as 70 types of descriptive types of information were defined, e.g.: earthquake name, location, magnitude, peak ground acceleration, thickness of the liquefied layer, ground slope, observed displacement magnitude, etc. The various displacement vectors and site investigation points at one event are combined, giving a mean and standard deviation for these parameters.

Using a multi-linear regression analysis the compiled data was used to set up a model to predict the magnitude of the horizontal displacement. Since not all descriptive information was available at all sites, a rough-to-fine model set-up was used as presented in figure 3.5.

- If only moment magnitude, fault rupture distance, peak ground acceleration and strong motion duration are known, a prediction of the horizontal displacement can be made using the regional component of the model. For this model 71 complete case studies were available yielding a moderate coefficient of determination  $R^2 = 0.537$ .
- If also the length of the sliding area, slope of the ground surface and the free face height are known, the site component of the model can be used, in combination with the regional component. For this model 58 complete cases were available yielding an  $R^2 = 0.710$ .
- If too the depth to the minimum safety factor of liquefaction and the depth to the liquefied layer itself are known, the geotechnical component of the model can be used, in combination with the site- and regional components. For this model 45 complete cases were available yielding an  $R^2 = 0.752$ .

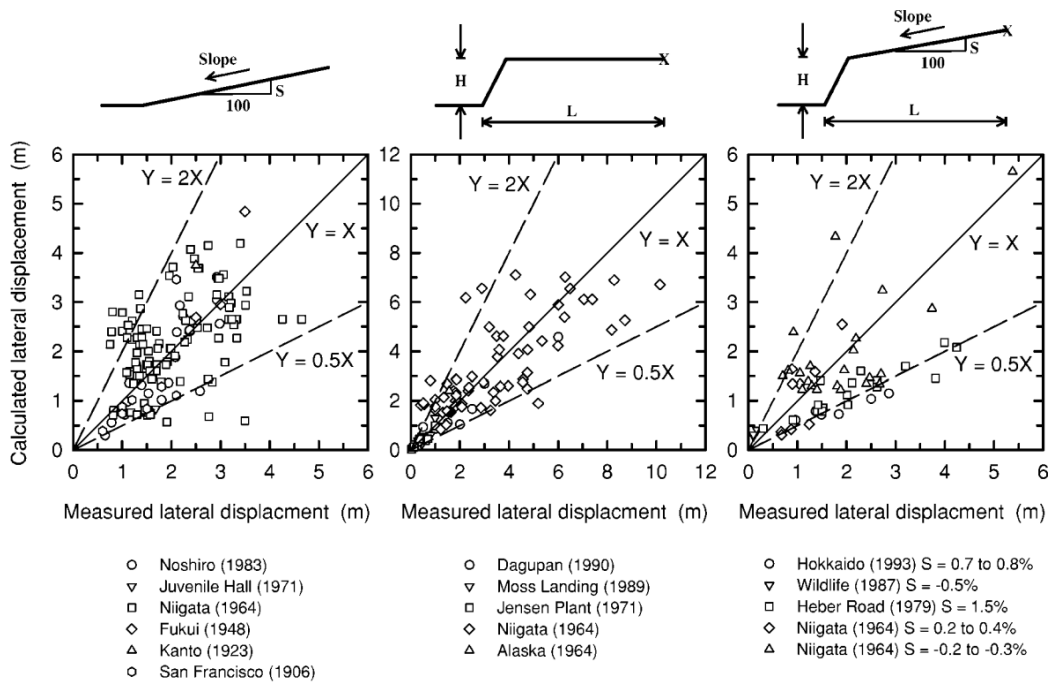
Figure 3.5 Overview of EPOLLS model for predicting the average and standard deviations of horizontal displacements [ref. 16]



Zhang et al. (2004) make an attempt to link the observed horizontal lateral displacement to a combination of a one-dimensional liquefaction severity index and simply geometric parameters. The severity index used is the Lateral Displacement Index (LDI) which is a depth-integrated measure of the (liquefied) strain potential of the soil column. The geometric parameter is either the slope  $S$  in absence of a free-face and the ratio  $L/H$  for free-face conditions. Herein  $H$  is the free-face height and  $L$  the distance behind the toe of the slope in meters. For verification of this procedure 13 case histories during 12 earthquakes are used. A selection procedure was used to exclude cases that were not 'purely' lateral spreading because of e.g. impeded displacements by boundary effects, multiple possible failure mechanisms, high static shear stresses that may have caused local slump and/or flow failure.

Unlike Rauch (1997) again the individual displacement vectors were used to assess the proposed model performance. The model performance is shown in figure 3.6 where it is noted that the two free-face datasets on the right are eventually combined which appears to be justified for slope up to 0.5 %.

Figure 3.6 Comparison of measured and calculated lateral displacements [ref. 34]



Valsamis et al. (2010) performed a variety of dynamic numerical analyses in FLAC using a material model that allows for the generation of excess pore pressures and thus the onset of liquefaction. The numerical model is calibrated by back-calculating centrifuge tests after which parameter variation studies are performed. The results from the latter are then regressed to obtain empirical relations that can be used to estimate horizontal displacements. Such procedure is similar to that of Bray (2016) to determine foundation settlements under the combined influence of earthquake loading and (partial) liquefaction.

$$D_H = 2.1 \left( \frac{a_{mean}}{g} \right)^{0.5} [T(N_{cyc} - N_L)]^{0.8} [(N_1)_{60,cs}]^{-1} [H_{tot}] [\tan i]^{0.5} (1 - FC)^3$$

Herein:

$a_{mean}$  is the mean acceleration in an acceleration time history in  $g$  ( $=9.81 \text{ m/s}^2$ ) which ranges between about 0.1 for a single significant cycle and 0.63 for a sinusoidal signal

$T(N_{cyc} - N_L)$  is the duration of strong shaking after initial liquefaction in seconds

$(N_1)_{60,cs}$  is the clean-sand corrected normalized SPT blow count of the liquefied layer [-]

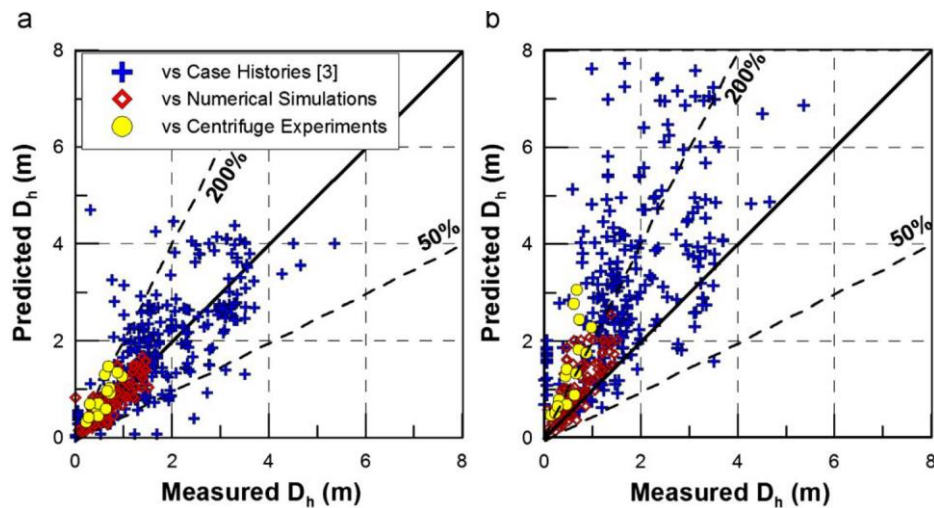
$H_{tot}$  is the depth to the sliding plane in m

$i$  is the ground surface inclination in degrees

$FC$  is the fines content of the liquefied layer in %

The performance of this relation is compared with the relation proposed by Hamada (1999) for several case histories, centrifuge experiments and the numerical simulations. For the case histories several assumptions were made for the missing parameters. In figure 3.7 it can be observed that this in general appears to yield a less conservative result. The prediction capability on first sight (using calculated versus measured diagrams such as figure 3.6) appears to be similar to the model by Youd et al. (2002), Rauch (1997) and Zhang et al. (2004).

Figure 3.7 Accuracy of predicted ground surface displacement from case histories, centrifuge tests and numerical simulations from (a) the relation by Valsamis et al. (2010) and (b) the relation by Hamada (1999)



### 3.3 Synthesis

Most prediction equations were derived for- or validated by observed displacements at strong tectonic earthquakes. Therefore they should not be applied directly to induced earthquakes in Groningen without verifying the background and validity ranges for which the prediction equations were derived. An example is the duration of induced earthquakes in Groningen which differs significantly from tectonic earthquakes, while the duration is not always present as a parameter in a prediction equation. In this section results and different aspects of the various methods presented in section 3.2 will be discussed.

#### 3.3.1 Applicability

##### Free field vs sloping ground

An overview of the applicability to free field and gently sloping ground conditions is given in table 3.1. The simplified procedures proposed by Hamada et al. (1986) and Hamada (1999) and the numerical study by Valsamis et al. (2010) are applicable only to gently sloping ground conditions. The procedure by Rauch (1997) is applicable for both, but does not make a distinction between the two conditions when calculating the magnitude of the horizontal displacement, the free face height is simply set to 0 in the case no free face is present.

Table 3.1 Applicability of methods for free face and gently sloping ground conditions

method	Free face	Gently sloping ground
Hamada et al. (1986)		x
Hamada (1999)		x
Youd et al. (2002)	x	x

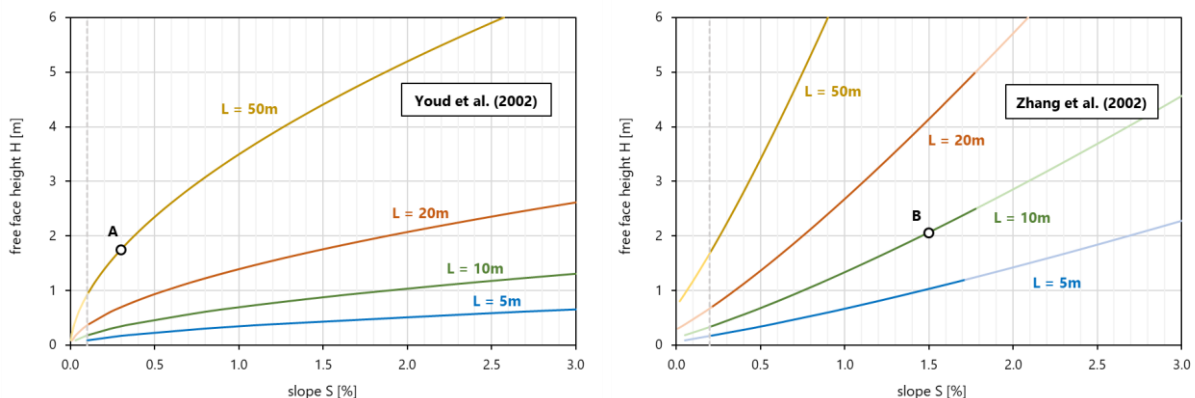
method	Free face	Gently sloping ground
Rauch (1997)	x	x
Zhang et al. (2004)	x	x
Valsamis et al. (2010)		x

Youd et al. (2002) and Zhang et al. (2004) both make a distinction between the conditions, albeit in a slightly different manner. In both methods the displacement expressions can be equalled to obtain a direct relation between free facing and sloping ground conditions. This is shown in figure 3.8 wherein on the left the equal-displacement curves by Youd et al. (2002) are presented and on the right those by Zhang et al. (2004). Here L is the horizontal distance from the toe of the slope at which the displacement is considered (see figure 3.6).

As these curves may be somewhat abstract, the meaning is illustrated by considering points A and B:

- Point A shows that at a free face height of 1.75 meters, the expected horizontal displacement at a distance of 50 meters behind the toe, is equal to the horizontal displacement of a gentle slope of 0.30 %, given the same geotechnical and seismic boundary conditions, using the procedure Youd et al. (2002).
- Point B shows that a free face height of 2.06 meters, the expected horizontal displacement at a distance of 10 meters behind the toe, is equal to the horizontal displacement of a gentle slope of 1.50 %, given the same geotechnical and seismic boundary conditions (expressed by the lateral displacement index), using the procedure by Zhang et al. (2004).
- Both points do not tell anything about the magnitude of the equal displacement.

Figure 3.8 Slope steepness versus free face height for Zhang et al. (2004) and Youd et al. (2002) relations



The validity of both equalities is bounded and presented by the bright coloured parts of the curves. The bounds can be expressed as follows:

- Youd et al. (2002):
  - For slopes the proposed procedure is valid in the range  $0.1 \% \leq S \leq 6.0 \%$ .
  - For free facing conditions the proposed procedure is valid in the range  $1 \% \leq H/L \cdot 100 \leq 20 \%$ .
- Zhang et al. (2004):
  - For slopes the proposed procedure is valid in the range  $0.2 \% \leq S \leq 3.5 \%$ .
  - For free facing conditions the proposed procedure is valid in the range  $4 \leq L/H \leq 40$ .

It can be observed that the shape of these curves differs significantly for slopes larger than about 0.5 %.

### Input parameters

The relation by Hamada (1986) is relatively easy and therefore easy to obtain a crude approximation of the displacement. However, for understanding whether lateral spreading is likely to occur the number of input parameters is too limited. The procedure by Hamada (1999) is more sophisticated and for this an acceleration time history at surface level is required. As the duration of shaking at a certain intensity is

included herein, this allows for an estimation of the displacement at shorter durations. Textually it is specified that the mean magnitude of the acceleration should be applied, but by back-calculating some of the presented results it appears that the maximum acceleration  $A_i$  per acceleration time history segment is used. The adopted definition of corrected overburden pressure  $\bar{N}$  is defined differently, but numerically comparable to  $(N_1)_{60}$  and thereby relatable to a certain relative density.

The relation by Youd et al. (2002) is scenario specific as the magnitude  $M$  and horizontal fault distance  $R$  have a significant effect on the outcome. Franke & Stewart (2014) propose a method to add the weighted contributions of all possible earthquake scenario's, similar to what is adopted in the Groningen Ground motion model, to reduce the sensitivity to variations herein. To be able to use the proposed equations a depth-accumulated thickness of granular layers with  $(N_1)_{60}$  is required. Using correlations an estimation of these values, as well as the estimated fines content in these layers, can be obtained from Cone Penetration Tests (CPTs).

The method proposed by Rauch (1997) yields larger displacements with increasing  $M$  and smaller displacements with increasing  $R$ . This makes sense: the stronger the earthquake and the closer one is to the source, the larger the expected displacements. However, through the multi-variate regression analysis smaller displacements are predicted with increasing maximum acceleration and duration. Although acknowledged, it is stated that this does not have an adverse effect on model outcome. This observation does however imply that the model can only be used to obtain an approximate value of the displacement, it is harder to perform a sensitivity analyses.

To include the site component, the expected length of the sliding plane is required, which is a difficult parameter to know a-priori. One can imagine that the closer to the free face, the larger the expected displacement as observed in figure 3.8. This behaviour is however not obtained by adopting the method by Rauch (1997) as a larger displacement is predicted if the lateral spread length is larger too.

Rauch (1997) states that by increasing the amount and detail of data the regression performance is increased, as can be shown from left to right in figure 3.9. However, if the database is limited and only all cases are considered at which all information is available, it is shown in figure 3.10 that model performance in terms of the regression coefficient  $R^2$  increases only marginally.

Figure 3.9 EPOLLS model performance as reported, from left to right including the regional-, site- and geotechnical component using all cases at which each type of data is available

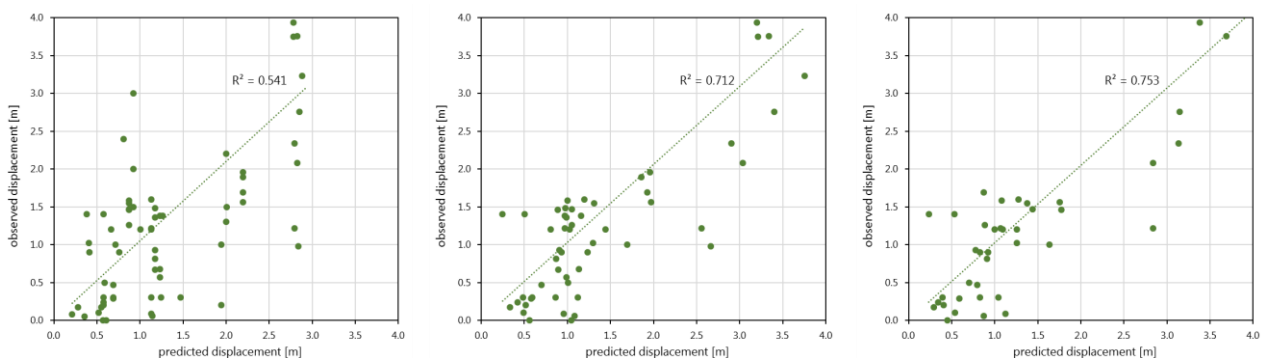
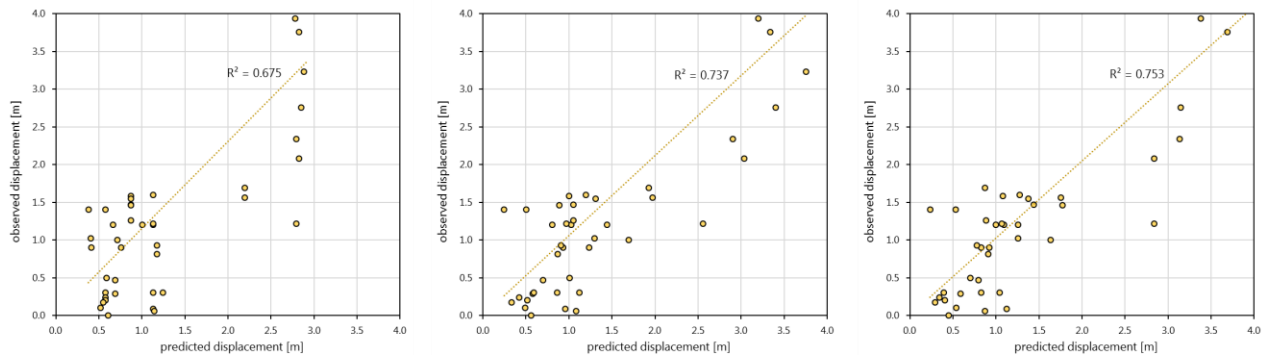
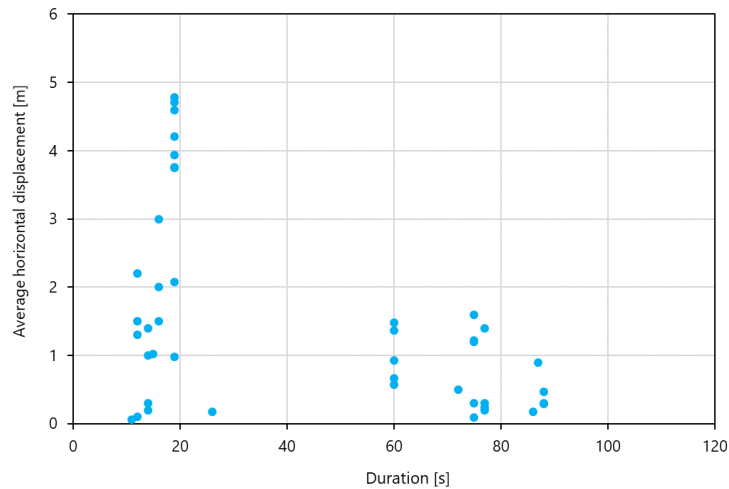


Figure 3.10 EPOLLS model performance from left to right including the regional-, site- and geotechnical component using only cases where all data is available



The procedure proposed by Zhang et al. (2004) has as an advantage that the accumulated liquefaction susceptibility of the soil profile is accounted for consistently. Moreover, the Groningen-specific triggering procedure by Green et al. (2018) can be adopted. In such procedure the duration is present through the magnitude safety factor *MSF* which accounts for the generation of excess pore pressures on a granular scale. On a global level only geometric aspects determine the ratio *LDI/LD* and inertia of the sliding mass is not taken into account. Given the non-apparent trend of lateral spreading displacement magnitudes with duration obtained from the database by Rauch (1997) (see figure 3.11) this may indeed seem as an obsolete parameter for strong tectonic earthquake case histories. It may however be essential for applicability to shorter duration earthquakes in Groningen.

Figure 3.11 Average horizontal displacement and (estimated) duration for cases in the database by Rauch (1997)



### 3.3.2 Indicative results for Groningen conditions

In this paragraph the output of the considered methods is evaluated. Based partially on available *LPI<sub>ISH</sub>* screening maps performed for the Groningen field, a case is selected in which both the liquefaction potential of the soil profile and the seismic load are relatively high. No attempt is made to quantify exactly how high, but it is emphasized that the results not necessarily represent the worst-case condition for the entire region and serve to illustrate typical outcomes for the different methods.

In **Fout! Verwijzingsbron niet gevonden.** all required input parameters per method are presented. It is noted that herein only the regional component from the method by Rauch (1997) is considered as the length of the lateral spread area is not a-priori known. Moreover, from the comparison between figure 3.9 and

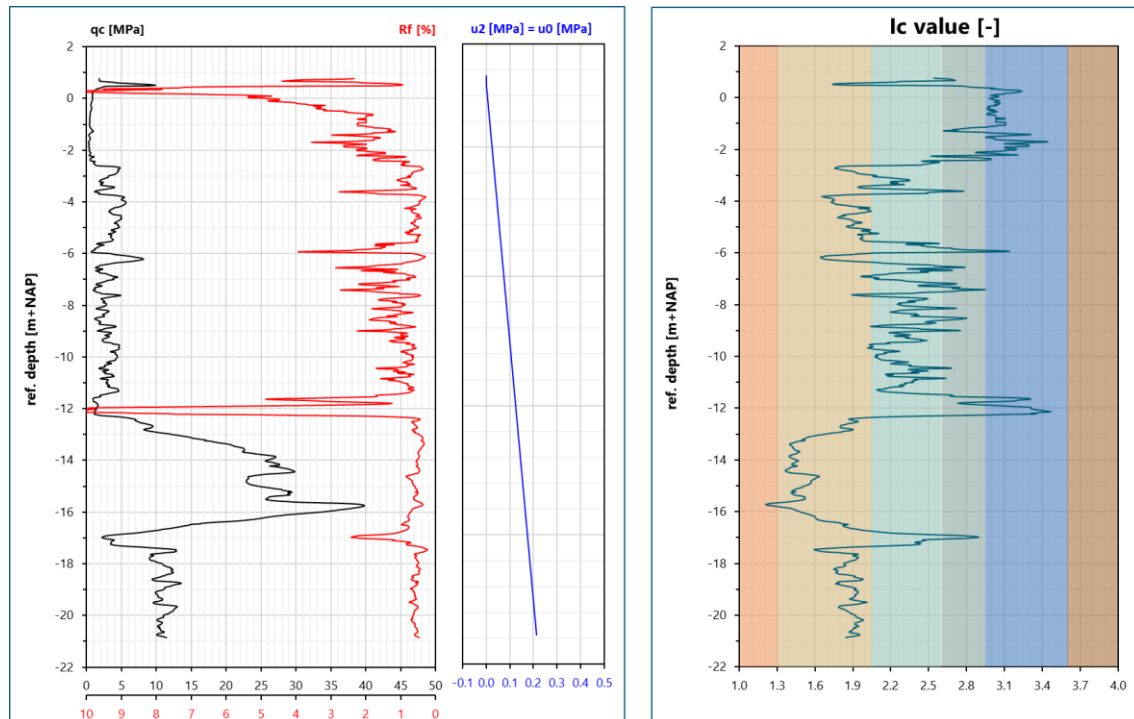
figure 3.10 it was concluded that including the site- and geotechnical components do not increase the prediction accuracy significantly.

Table 3.2 Required input parameters for each method

	Symbol	Explanation	Hamada et al. (1986)	Hamada (1999)	Youd t al. (2002)	Rauch (1997)	Zhang et al. (2004)	Valsamis et al. (2010)
load parameters	M	earthquake magnitude			x	x	x	
	R	rupture distance			x	x		
	a(t)	acceleration time history		x		x		x
	$a_{max}$	maximum acceleration				x	x	
geometry	$S$	slope	x	x	x	x	x	x
	$H$	free face height			x	x	x	
geotechnical	$H_{liq}$	liquefied layer thickness	x	x				x
	$N(z)$	depth-dependent site investigation (SPT/CPT)		x	x		x	x
	$F_{15}$	finer content (at $N < 15$ )			x			x
	$D50_{15}$	mean grain size (at $N < 15$ )			x			

For representation of the soil conditions site investigation profile CPT48436 is selected, which is located near Westeremden. The depth profile is presented in figure 3.12 at which it is assumed that the phreatic level lies 50 cm below ground surface level. The peak ground acceleration  $a_{max}$  for the 1/2,475 return period at this location is 0.20 g (V5, T1) and is situated in cluster C which is relevant for the applicable time histories (see NPR 9998 webtool for the definitions of V5, T1 and clusters).

Figure 3.12 Soil profile CPT48436



For the comparison of methods two hypothetical geometric cases will be considered:

- A (semi-)infinite slope with a steepness  $S$  of 1 %.
- A free-facing 1:3 slope with a height  $H$  of 3 meters.

With respect to the other required input parameters from **Fout! Verwijzingsbron niet gevonden.** the following is noted:

- $M$  is the earthquake moment magnitude. The seismic loads from the NPR9998 webtool are the result of many scenarios and thus possible values of  $M$  (in combination with rupture distance  $R$ ) and the value of  $M$  can therefore not be directly compared to a specific acceleration time history  $a(t)$  or  $a_{max}$ . A value of  $M = 5$  is selected as this value is adopted in the liquefaction analysis.
- $R$  is the rupture distance for which an arbitrary value of 1 km is chosen.
- $a(t)$  is acceleration time history, of which  $a_{max}$  is the absolute maximum. For the selected location  $a_{max} = 0.20g$  according to the NPR9998 webtool. For the definition  $a(t)$  the acceleration time histories that belong to cluster C are used:
  - In the procedure by Rauch (1997) the strong shaking duration is defined as the total duration between the first and last exceedance of 0.05g. The average from the 22 time histories (11 in both x and y direction) that belong to cluster C in this case is 4.2 seconds. For the scaling of the signals  $\gamma_l$  and  $\gamma_n$  are set equal to 1.
  - Valsamis et al. (2010) adopt the parameter  $T(N_{cyc} - N_L)$  defined as the duration of strong shaking after the onset of liquefaction. Since determining this parameter based on a simplified analysis is not possible, for this parameter the same definition from Rauch (1997) is adopted. The mean acceleration  $a_{mean}$  is taken as the average of the absolute accelerations during these periods of strong shaking and the average over the 22 time histories is equal to 0.043 g.
  - The averaged cumulative term  $\sum_i^n A_i^{0.48} T_i$  in the method by Hamada (1999) for the 22 time histories is equal to 40.1 where for the time intervals  $T_i$  the time steps of the signals are used.
- $H_{liq}$  is the thickness of the liquefied layer, for which the cumulative thickness of all layers with  $FS_{liq} < 1$  is calculated, using the liquefaction procedure by Green (2018) in the NPR9998, which results in a total thickness of 3.2 meters. In the procedure by Valsamis et al. (2010) the parameter  $H_{tot}$  is used, which is defined as the total thickness of the layer above the sliding plane, which does not necessarily liquefy as a whole. The value of  $H_{tot}$  is in this case 6 meters.
- $N(z)$  is the in-situ depth-dependent measurement of the liquefaction resistance:
  - For the procedure by Zhang et al. (2004) it is needed to calculate the depth-integrated strain potential of the soil. The lateral displacement index LDI is 88.6 cm using Eq. (85) by Idriss & Boulanger (2008) and 52.9 cm using the equations proposed by Zhang et al. (2004). The cause of this notable difference between these methods which are essentially based on the same data, is not investigated, both values will be presented.
  - For the procedure by Youd et al. (2002) it is needed to determine the cumulative thickness of layers with a normalized SPT blow count lower than 15 (or  $D_R < 57\%$ ) which is in this case 5.2 meters;
  - for the procedure by Hamada (1999) and Valsamis et al. (2010) this is needed to determine the (averaged) normalized SPT blow count of the liquefied layer which is in this case equal to 11.6.
- $F_{15}$  and  $D50_{15}$  are respectively the fines content and the median grain size diameter of the cumulative subsoil fraction with SPT blow count below 15. Based on the  $I_c$  relationship adopted in the liquefaction triggering procedure by Boulanger & Idriss (2015) (that substantiates the triggering procedure by Green (2018)) the value of  $F_{15}$  is equal to 37 %. For  $D50_{15}$  a value of 150  $\mu m$  is assumed. For the procedure by Valsamis et al. (2010) the (averaged) fines content of the actually liquefied layer should be taken, which is 29 % based on the liquefaction triggering procedure by Green (2018).

Table 3.3 Horizontal displacement magnitudes for different considered methods

method	Free face (20 meters behind the toe)	Gently sloping ground
Hamada et al. (1986)	-	134 cm
Hamada (1999)	-	11 cm
Youd et al. (2002)	4 cm	3 cm

method	Free face (20 meters behind the toe)	Gently sloping ground
Rauch (1997)	24 cm	24 cm
Zhang et al. (2004)	70 - 117 cm	64 - 107 cm
Valsamis et al. (2010)	-	3 cm

The results in table 3.3 indicate a large spread in outcomes, which is partially due to the fact that the inserted input parameters are beyond the range for which the methods were derived. However, using above values some important remarks can be made:

- The results by Hamada et al. (1986) and Zhang et al. (2004) are by far the largest, which is likely due to the fact that there is no inertia/duration term and thus the values that are calculated only make sense if they are applied to earthquakes which similar characteristic to those in the database.
- The 24 cm displacement calculated by Rauch (1997) consists for more than half of the constant 14.9 cm, which may be acceptable at displacement magnitudes of several meters, but will dominate the calculated displacement at lower displacement magnitudes.
- The displacements calculated by Youd et al. (2001) are small, but very sensitive to slight changes in magnitude  $M$  as the expected displacement magnitudes nearly double if  $M = 5.2$  is taken rather than  $M = 5.0$ . The fines content too has a strong influence; if  $FC = 23\%$  is used instead of  $FC = 37\%$ , the expected displacement doubles as well. Estimation of the fines content is in this case based solely on CPT and therefore introduces a significant uncertainty, see Boulanger & Idriss (2015).
- The methods by Hamada (1999) and Valsamis et al. (2010), both using the acceleration time history, predict relatively small displacement magnitudes compared to the other methods. The predicted displacement from the procedure by Hamada (1999) is smaller than from the procedure by Valsamis et al. (2010) which is in agreement with their findings as shown in figure 3.7. In their method the fines content is a very dominant parameter, both through the parameter  $(N_1)_{60,cs}$  and by applying a third power to the term  $(1 - FC)$ .

### 3.3.3 Liquefaction susceptibility

The precondition of lateral spreading is in all cases the occurrence of liquefaction. Moreover, predicted displacement magnitudes of several centimeters at large distances do require that the liquefied layer is continuous horizontally. Youd (2018) notes that for liquefied layers with thickness less than 30 cm, CPT methods generally result in an overprediction of lateral displacement. In a deltaic regions such layers are seldomly continuous and the measured CPT data becomes less accurate.

One of the aspects that is missing from the databases is the inclusion a very small magnitude lateral spread displacements. In general, the case history database contains mainly cases in which large displacements were found, after which site investigations were performed. There are very few cases in which no displacement was observed, where in reality large displacements were to be expected. One of these cases is found in Turkey during the 1999 Kocaeli earthquake [ref. 31] and it touches on the same issue often encountered in Groningen: the liquefaction susceptibility of layered and interbedded soils.

Boulanger et al. (2016) investigate in closer detail the discrepancy between the estimated 1D-CPT-based horizontal displacement and the absence thereof in reality. For a matching analysis result it is concluded that a correction for transition- and thin layers effects alone (and site-specific fines calibration) is not sufficient. By also accounting for the horizontal spatial variability of the soil layers and adopting a 2D-non-linear analysis procedure, more satisfying results are found.

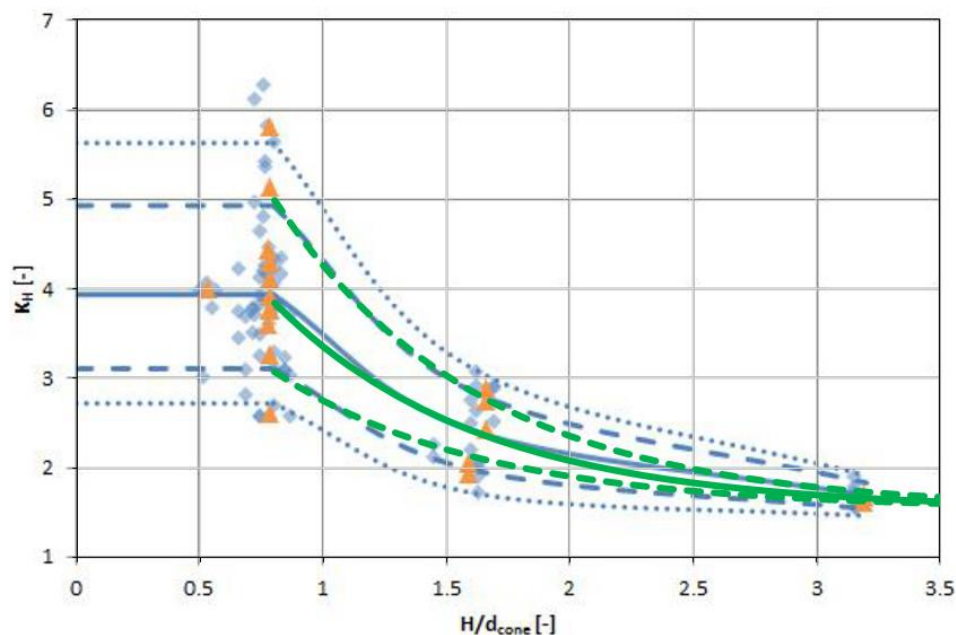
In practice these two last steps require significant soil investigation and calculation capacity. By adopting the transition- and thin layer corrections the bias of the outcome is reduced (improved) and recently advances have been made to adopt larger correction factors than the often referred to maximum of 1.8 by Youd et al. (2001). Boulanger & DeJong (2018) propose an inverse-filtering procedure in which correction factors up to a factor of 3 can be found, depending on the normalized thickness of the thin layers that require correction.

Greef & Lengkeek (2018) proposed to use a simpler spreadsheet-based correction procedure, based on the equation by Youd et al. (2001). The correction factor  $K_z$  applied to an interbedded layer herein is a function of the smallest vertical distance  $z$  to a cohesive layer either on top- or below the interbedded layer.

$$K_z = 1 + 0.25 \left( \frac{1}{17} \left( \frac{2z}{d_c} \right) - 1.77 \right)^2$$

Lange (2018) performed multiple laboratory tests at three different  $H/d_{cone}$  ratios, of which the aggregate results are presented in figure 3.15. These results imply that at small  $H/d_{cone}$  ratios a maximum correction of 1.8 is not justified and higher values could be adopted. To apply these results in CPT analyses in Groningen, an approximate curve fit is made, that can be used in addition to the equation for  $K_z$  presented above.

Figure 3.13 Derived correction factors as function of the H/d ratio [ref. 21]. The blue curves connect the mean (solid), 15 % upper- and lower bound (striped) and 5 % upper- and lower bound (dotted) values at the three H/d ratios investigated. The green curves present the proposed relation to be implemented in spreadsheet liquefaction analyses for small  $H/d_{cone}$  ratios



For values of  $H/d_{cone} \leq 4$  the following empirically fitted equation is proposed in which  $\Phi^{-1}$  is the inverse of the standard cumulative normal distribution and  $P$  is the exceedance probability. The curves for  $P = 15\%$ ,  $50\%$  and  $85\%$  are plotted in figure 3.15 giving a reasonable approximation of the curves by Lange (2018). At  $H/d_{cone} = 4$  the value of  $K_z$  at  $P = 50\%$  is exactly equal to the equation of  $K_z$  based on the recommendation by Youd et al. (2001).

$$K_z = 1.54 + 6.0 \exp \left\{ 0.39 \cdot \Phi^{-1}(P) - 1.2 \left( \frac{2z}{d_c} \right) \right\}$$

The results after implementing the described thin layer correction to CPT 48436 are presented in table 3.4.

By comparing to the results in table 3.3 the following remarks are made:

- The liquefied layer thickness decreases  $H_{liq}$  slightly to 2.7 meters and the relative density of the liquefied layer increases to 52 % and the cumulative thickness at which  $D_R < 57\%$  decreases from 5.2 to 3.2 meters.
- Above results in a decrease in predicted horizontal displacement for the methods by Hamada et al. (1986), Hamada (1999) and Zhang et al. (2004) although these reductions are not very significant.
- The methods by Youd et al. (2001) and Valsamis et al. (2010) show an increase in predicted displacement. As the cone resistance increases after correction, the predicted fines content decreases as the value of  $I_c$

changes. If for those layers  $FS_{liq}$  does not significantly increase thereby reducing  $H_{liq}$ , the reduction in predicted fines content outweighs the effect of the reduced liquefied layer thickness.

Table 3.4 Horizontal displacement magnitudes for different considered methods - after thin layer correction (percentages between brackets show the difference compared to table 3.3)

method	Free face (20 meters behind the toe)	Gently sloping ground
Hamada et al. (1986)	-	123 cm (-8 %)
Hamada (1999)	-	9 cm (-18 %)
Youd et al. (2002)	6 cm (+50 %)	4 cm (+33 %)
Rauch (1997)	24 cm (--)	24 cm (--)
Zhang et al. (2004)	51 - 85 cm (-27 %)	46 - 78 cm (-27 %)
Valsamis et al. (2010)	-	4 cm (+33 %)

These findings indicate that although transitional- and thin layer corrections can help to reduce the predicted liquefaction susceptibility, in predicting the consequences of liquefaction these corrections may be less helpful. This partly is a consequence of the fact that semi-empirical relations with a strong substantiation in case history data, do not always give reasonable or satisfactory results on a marginal level as was observed for the duration and PGA in the procedure by Rauch (1997).

### 3.3.4 Combination of methods

As mentioned in paragraph 3.3.1 all available methods have their limitations which introduces a non-quantified uncertainty when applying them to Groningen conditions. In this paragraph different aspects of the methods are combined to overcome the most important limitations and a relation is obtained that gives seemingly reasonable results for Groningen conditions. As will be discussed hereafter, the results are still prone to great variability and are not verified using Groningen specific case history data. Therefore they should only be used to obtain an indicative displacement magnitude if the subsoil is indeed believed to be prone to liquefaction (see introduction in section 3.1).

The following aspects were considered:

- Displacements for (semi-)infinite, sloping ground can be obtained by applying either the method from Hamada (1999) or the proposed procedure by Valsamis et al. (2010). Both use the acceleration time history, rather than moment magnitude and epicentral distance:
  - The horizontal displacement from the method by Hamada (1999) is herein called  $D_{H;1}$ .
  - Rather than using  $\bar{N}$  it is more insightful to use the relative density  $D_R$  as an input parameter. The definition for  $\bar{N}$  by Hamada (1999) is numerically nearly equal to the normalized SPT blowcount  $(N_1)_{60}$ . By adopting the relation by Idriss & Boulanger (2008) between the normalized SPT blowcount and relative density, the factor  $\bar{N}^{0.88}$  is approximately equal to  $D_R^{1.76}/114$  where  $D_R$  is in percent.
  - The horizontal displacement from the method by Valsamis et al. (2010) is herein called  $D_{H;2}$ .
  - As stated in paragraph 3.3.2 for the strong duration after the onset of liquefaction, the strong shaking duration  $D$  as defined by Rauch (1997) is used.
  - In general for the considered slopes it holds that  $i \ll 1$ , implying  $\tan i \approx i$ , and with  $i = S/100$  it thus holds that  $[\tan i]^{0.5} \approx \sqrt{S}/10$ .

$$D_{H;1}(S_{Y,Z}) \approx \frac{\sqrt{H_{liq}} \cdot S_{Y,Z}}{0.7 D_R^{1.76}} \cdot \sum_i^n A_i^{0.48} T_i$$

$$D_{H;2}(S_{Y,Z}) \approx \frac{\sqrt{a_{mean}} \cdot D^{0.8} \cdot H_{tot} \cdot \sqrt{S_{Y,Z}} \cdot (1 - FC)^3}{0.0219 \cdot D_R^2}$$

- As shown in figure 3.8 the methods by Youd et al. (2002) and Zhang et al. (2004) provide a relation between a combination of free face height  $H$  and distance  $L$  and the ground slope.  $S_Y$  is the equivalent slope that results in the same free field displacement as a function of  $H$  and  $L$ , according to the method by Youd et al. (2002).  $S_Z$  is the equivalent slope that results in the same free field displacement as a function of  $H$  and  $L$ , according to the method by Zhang et al. (2004).

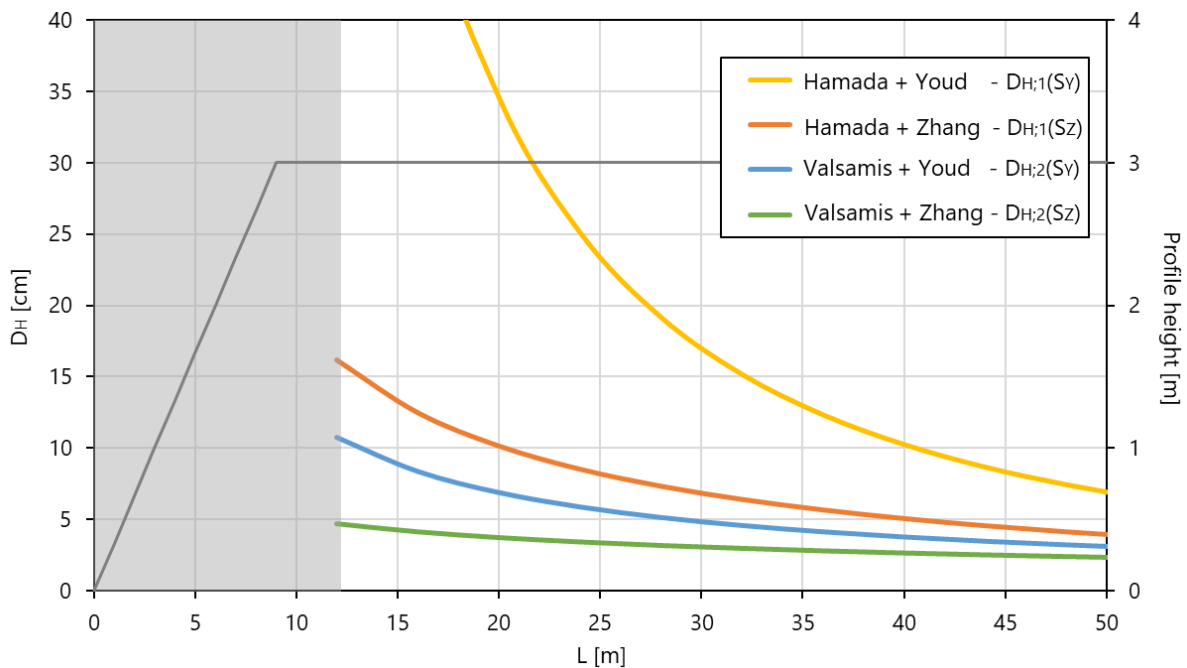
$$S_Y = 10^{\frac{0.592}{0.338} \log\left(\frac{H}{L-100}\right) - \frac{0.5}{0.338}}$$

$$S_Z = 6 \left(\frac{L}{H}\right)^{-0.8} - 0.2$$

By combining the above, four different relations are obtained, defining the horizontal displacement  $D_H$  as a function of geotechnical-, seismic loading- and geometrical parameters.

For the same case study conditions as in paragraph 3.3.2, and by applying the thin-layer correction presented in paragraph 3.3.3, for the above four combined methods the horizontal displacements are shown in figure 3.14. These are a function of the horizontal distance from the toe of the slope  $L$  with a fixed free face height  $H$  of 3 meters. Herein the grey area indicates the  $L/H = 4$  boundary below which lateral spreading is no longer the predominant phenomenon according to Zhang et al. (2004). Note that Youd et al. (2002) effectively use  $L/H = 5$  as a validity boundary. The horizontal projection of the slope (= 9 meters) is included in the parameter  $L$  and a value of 20 meters thus implies considering the horizontal displacement 11 meters behind the slope.

Figure 3.14 Horizontal displacement as a function of  $L$  for the 4 combined methods. The grey line indicates the slope geometry of which the height is presented on the secondary vertical axis



At a distance of 20 meters and the predicted horizontal displacement varies from 4 - 35 cm among the methods. Although dependent on the different input parameters, the predicted displacements by Valsamis et al. (2010) are generally lower than by Hamada (1999), unless the fines content is very low. This is not an explicit parameter in the latter method.

Significantly the largest displacements are predicted by  $D_{H,1}(S_Y)$  in particular at relatively short distances  $L$ . This observed exponential increase is caused by a combination of two factors:

- $S_Y$  inflates (far beyond the validity range of 6 %) for large ratios of  $H/L$  in combination. This is also visualised by the near-horizontal curves in the left side figure 3.8 for decreasing  $L$ .
- The displacement predicted by the method from Hamada (1999) depends linearly on  $S$ .

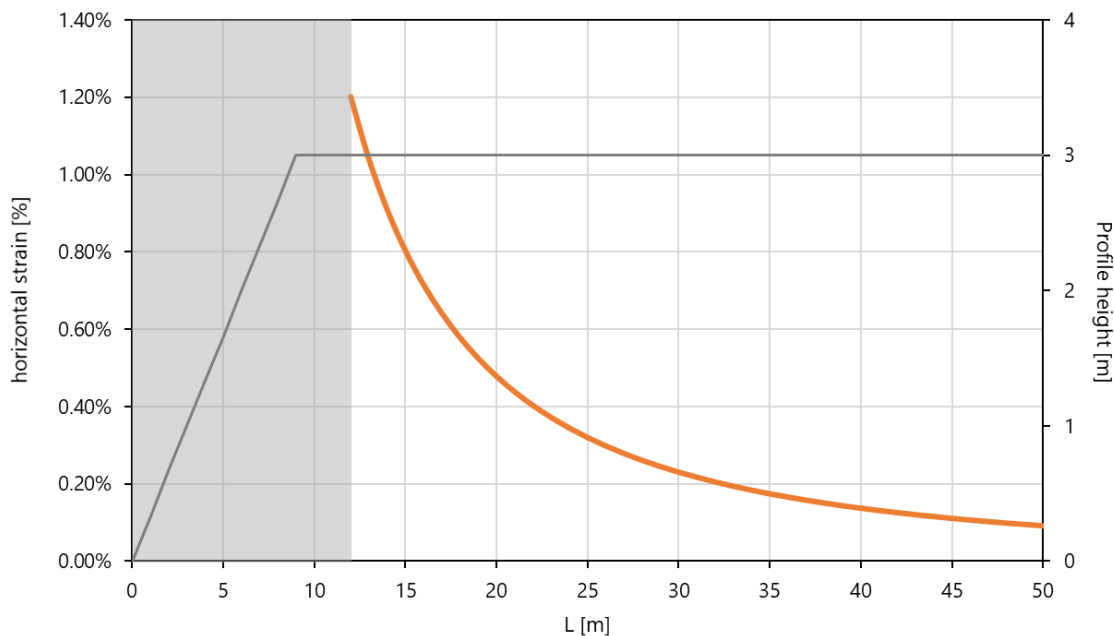
The calculated displacements are relatively low compared to the general absolute prediction accuracy of the methods in e.g. figure 3.6, figure 3.7 and figure 3.9. They do however provide an indication to obtain displacements that feel more in place for Groningen conditions and short durations earthquakes. For a preliminary assessment of the lateral spread displacement it is recommended to use  $D_{H;1}(S_Z)$  for the following reasons:

- It approximates the average of the four combined methods at  $L \geq 10H$ , while at smaller values of  $L$  it is not affected by the exponential increase of  $S_Y$ ;
- In terms of the choice between the method by Hamada (1999) and Valsamis et al. (2010) the former in this case is more conservative. There is however a smaller dependency on the (uncertain) fines content and CPT based thin layer correction will result in a marginal reduction of expected horizontal displacement, rather than an increase (see table 3.4).

It is difficult to provide a bandwidth as the total prediction uncertainty consists of several factors: prediction uncertainty of the reported models, uncertainty arising from combining two separate methods and uncertainty by applying this to Groningen conditions. Only the former can be quantified by using the fact that for most methods 90 % of the data falls within the 50 % to 200 % prediction bounds. As the methods attempt to give best estimates, it is assumed that the number of under- and overpredictions are equal. Then the prediction uncertainty can be described by multiplying  $D_H$  with  $\varepsilon$ , wherein  $\ln(\varepsilon)$  is normally distributed with mean 0 and a standard deviation of 0.42.

With respect to assessing the vulnerability of shallow- or pile foundations the horizontal displacement can too be expressed as horizontal strain, defined as  $D_H/L$  as varying intervals. The result hereof for  $D_{H;1}(S_Z)$  is presented in figure 3.15 which shows the horizontal strain as a function of  $L$ .

Figure 3.15 Horizontal strains as a function of  $L$  for the Westeremden case study, assuming a slope height  $H$  of 3 meters



Using  $D_{H;1}(S_Z)$  in table 3.5 the results of a limited sensitivity analysis is presented using two different locations, return periods and free face heights  $H$ .

- The first location is Westeremden at which CPT 48436 is used and of which most details are provided in paragraph 3.3.2. Additionally:

- $a_{max}$  at T = 975 years is 0.16 g,  $H_{liq} = 0.44$  m,  $D_R$  of the liquefied layer is 48 %.
- The second location is Tjuchem at which CPT 5012-0283-000\_DKMP2 is used (see figure 3.16). This location is in the V5 model zone with the highest horizontal peak ground accelerations, and too has a significant liquefaction potential. Hereafter a short summary of the analysis details is provided:
  - $a_{max}$  at T = 2,475 years is 0.25 g,  $H_{liq} = 2.20$  m,  $D_R$  of the liquefied layer is 57 %.
  - $a_{max}$  at T = 975 years is 0.19 g,  $H_{liq} = 2.08$  m,  $D_R$  of the liquefied layer is 56 %.

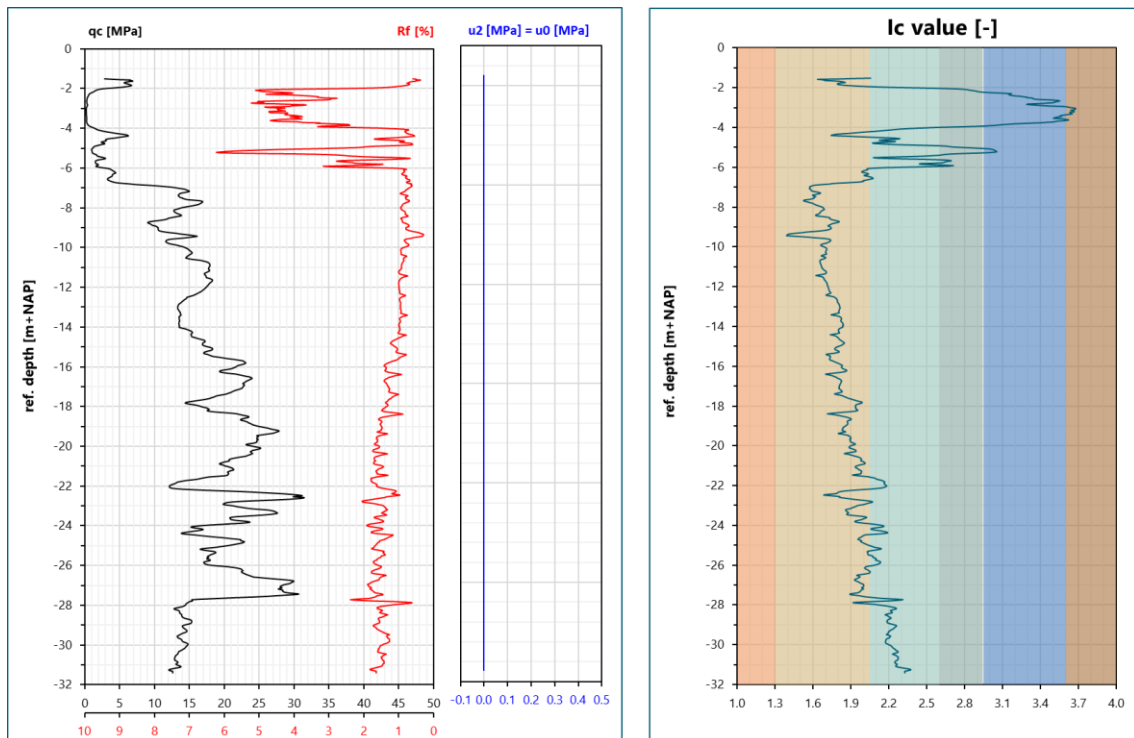
The displacement is evaluated at a distance  $L = 20$  meters behind the slope. The transitional- and thin layer corrections that will be discussed in paragraph 3.3.4 are implemented in the presented results (note that this causes the difference between the 9.8 cm in table 3.5 and the 11 cm in table 3.3).

Table 3.5 Calculated horizontal displacement at a distance  $L = 20$  meters from the toe of a fictive slope with height  $H$

	T = 2475 years		T = 975 years	
	H = 1 m	H = 3 m	H = 1 m	H = 3 m
CPT Westeremden	3.0 cm	9.8 cm	1.3 cm	4.2 cm
CPT Tjuchem	2.6 cm	8.3 cm	2.3 cm	7.3 cm

As expected from the functional form of  $D_{H,1}(S_z)$ , the free face height  $H$  has a near inverse linear effect on displacement. At Westeremden the difference in seismic demand between the return periods is very pronounced and the liquefied layer thickness reduces significantly at the reduced seismic demand. At Tjuchem the seismic demand at both return periods causes significant liquefaction, resulting in a less pronounced difference between the return periods.

Figure 3.16 Soil profile CPT5012-0283-000\_DKMP2



### 3.3.5 Geometrical considerations

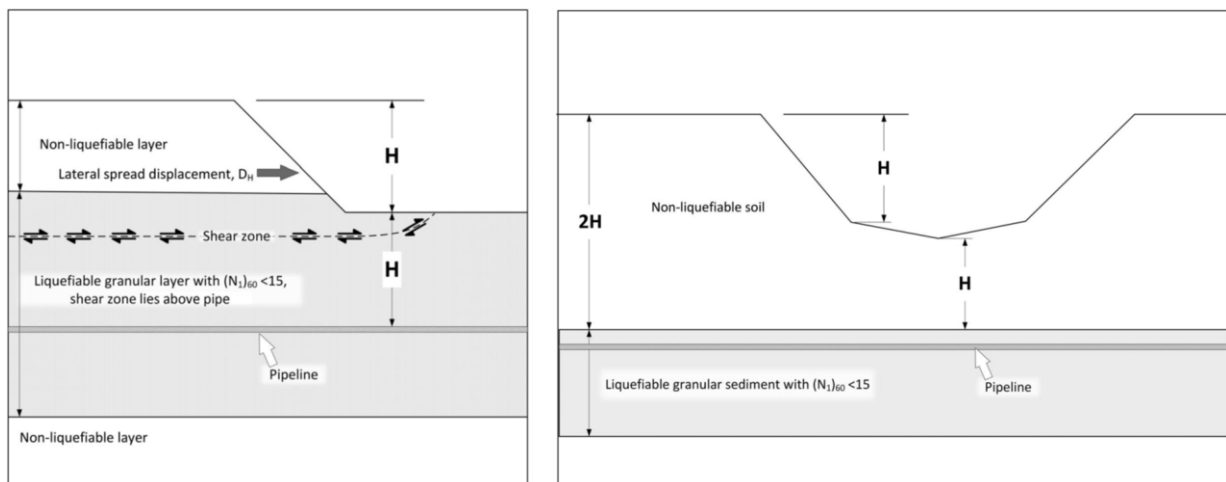
Apart from the limited presence of false positives in the lateral spreading databases, another aspect that is hardly addressed is the relative position of the liquefied layer compared to the free face. For a shallow ditch it feels very conservative to predict large lateral displacements if the potentially liquefiable layer is found several meters below the ditch. Youd (2018) from a consulting practice perspective, addresses this topic with respect to the question at which depth pipelines should be positioned in order to prevent damage.

Herein two situations are addressed:

- A liquefiable layer that extends more than  $H$  below the canal bottom of a wide canal (see left figure 3.17). For this situation it is suggested to position a pipeline at a depth  $H$  below canal bottom as it is most likely that a shear band will develop in the top of liquefied layer.
- A liquefiable layer that is located at a depth  $2H$  below the surface level with a coverage of  $H$  below the deepest point of the canal bottom (see right figure 3.17). For this situation it is suggested that, for a canal width less than about  $4H$ , the cover should have sufficient strength to prevent lateral spreading. The strength of this cover should however be verified through in-situ testing or laboratory testing.

In both cases it appears that only liquefaction in a zone of  $2 \cdot H$  below the surface level affects the lateral displacement magnitude. The only case that is not considered herein is a deep liquefiable layer near a wide canal. However, to avoid significant calculated lateral spread displacements near relatively small ditches and canals, applying a criterion as visualised on the right side of figure 3.17 would be a sensible first step. A measure of the strength should then however be quantified and the approximate width of  $4H$  verified.

Figure 3.17 Diagram of shallow (left) and deep (right) liquefiable layer and buried pipeline [ref. 32]



If applied to the analyses presented in paragraph 3.3.4 the calculated displacements from table 3.5 reduce to the values presented in table 3.6. Herein only the cumulative thickness of liquefied layers is accounted for in a zone of  $2 \cdot H$  below the surface level. As it can be observed, for all cases in which  $H = 1$  meter, the horizontal displacements are reduced to 0 cm. For the cases in which  $H = 3$  meters the results are more or less unaffected, only at Westeremden at  $T = 2,475$  years a slight reduction is observed as some liquefaction is predicted at a depth of  $2 \cdot H$  below surface level.

Table 3.6 Calculated horizontal displacement at a distance  $L = 20$  meters from the toe of a fictive slope with height  $H$ , including the relative position of the liquefied layer compared to the free face

	T = 2,475 years		T = 975 years	
	H = 1 m	H = 3 m	H = 1 m	H = 3 m
CPT Westeremden	0 cm	9.1 cm	0 cm	4.2 cm
CPT Tjuchem	0 cm	8.3 cm	0 cm	7.3 cm

### 3.4 Conclusions and recommendations

- In general lateral displacement magnitudes from international literature are predicted using semi-empirical relations that are substantiated by case history data from tectonic earthquakes. The functional form hereof may thus lead to significantly larger displacement than is likely for Groningen conditions.
- To determine the expected horizontal displacement at free facing conditions that are abundant in Groningen (and generally in the Netherlands), an assessment is made using two methods that rely on the acceleration time history rather than magnitude  $M$  and epicentral distance  $R$ . Since these methods are derived for gently sloping ground conditions with a slope  $S$ , in addition for two methods the slope is expressed as a function of free face height  $H$  and distance  $L$  using equal-displacement relations.
- The total of four combined relations were applied to a case study in which the liquefaction potential is relatively high (based on  $LPI_{SH}$  maps). The variety in outcome is significant, but for obtaining a first indication of the lateral spread displacement it is recommended to use specifically one of the four combined relations of which the expression is given below. The main reasons are consistency of predicted values at short distances from the slope and outcome sensitivity with respect to an often uncertain fines content.

$$D_H \approx \frac{\sqrt{H_{liq}} \cdot \left[ 6 \left( \frac{L}{H} \right)^{-0.8} - 0.2 \right]}{0.7 D_R^{1.76}} \cdot \sum_i^n A_i^{0.48} T_i$$

- As observed in above expression the precondition for lateral spreading is a liquefied layer with a certain thickness  $H_{liq}$ . For this purpose in the case study the cumulative thickness was adopted for layers where  $FS_{liq} < 1$ . This may be conservative depending on how discontinuous and/or interbedded the liquefied layers are. Adopting new insights on transitional- and thin layer corrections can partly reduce this conservative bias.
- The calculated displacement at a distance  $L$  is only applicable if a liquefied layer is continuous in horizontal direction which can only be established by a relatively dense site investigation.
- Given that the predicted liquefied layer thickness  $H_{liq}$  is significant and continuous in horizontal direction, there is no indication that lateral spreading cannot occur in Groningen. The proposed expression can be used to provide a first quantitative indication of the displacement magnitude, using local site investigation ( $H_{liq}, D_R$ ), geometry ( $H, L$ ) and seismic loading ( $a(t)$ ). The latter can be obtained through the NPR9998 webtool.
- **The relevance of lateral spreading to the Groningen region can be assessed by combining these seismic loading-, local site investigation- and geometry components.** The seismic loading component can be obtained through the GMM, the local site investigation component can be obtained from (automated) CPT analyses and for the geometry component an analysis within a GIS environment could be adopted.
- As the horizontal displacement is expressed as a function of the distance from the free face, it is possible to establish horizontal strain levels. To assess vulnerability of foundations and (infra-)structural objects to lateral spreading, it is recommended to couple these strains to the performance of these objects. This can be combined with a region-wide assessment of the relevance of lateral spreading, by zooming in on locations where significant lateral spreading displacements are expected.
- In the request for offer it was specifically asked whether lateral spreading may be expected for 'slightly larger' events. As this statement is not quantified, in this report two locations were evaluated with

significant liquefaction potential, using relatively high return periods. The conclusion is that lateral spreading can occur, albeit it rarely does because three conditions must be met in order to happen:

- A horizontally continuous loose sandy soil layer.
  - A relatively strong earthquake is required to induce liquefaction in this layer.
  - Relatively high slopes / deep water bodies.
- One technical aspect that is hardly addressed is the vertical position of the liquefied layer(s) relative to the free face height. A simple provision from literature is provided which may prove very helpful when assessing the many ditches and canals in Groningen that have a relatively small free face height.

### 3.5 References

- 1 Bartlett, S.F., Youd, T.L. 1992. Empirical Analysis of Horizontal Ground Displacement Generated by Liquefaction-Induced Lateral Spreads - Technical Report NCEER-92-0021.
- 2 Bartlett, S.F., Youd, T.L. 1995. Empirical Prediction of Liquefaction-Induced Lateral Spread. *Journal of Geotechnical Engineering*, Vol. 121, No. 4, pp. 316-329.
- 3 Boulanger, R.W., Idriss, I.M. 2015. CPT-Based Liquefaction Triggering Procedure. *Journal of Geotechnical and Geoenvironmental Engineering*, Vol. 142, No. 2.
- 4 Boulanger, R.W., Moug, D.M., Munter, S.K., Price, A.B., DeJong, J.T. 2016. Evaluating liquefaction and lateral spreading in the interbedded sand, silt and clay deposits using the cone penetrometer. *Australian Geomechanics*, Vol. 51, No. 4, pp. 109-128.
- 5 Boulanger, R.W., DeJong, J.T. 2018. Inverse filtering procedure to correct penetration data for thin-layer and transition effects. *Cone Penetration Testing 2018 - Keynote papers*, pp. 25-44.
- 6 BRANZ Seismic resilience. <http://www.seismicresilience.org.nz/topics/seismic-science-and-site-influences/earthquake-hazards/lateral-ground-displacement/>, accessed 29 August 2018.
- 7 Cubrinovski, M., Robinson, K., Taylor, M., Hughes, M., Orense, R. 2012. Lateral spreading and its impacts in urban areas in the 2010-2011 Christchurch earthquakes. *New Zealand Journal of Geology and Geophysics*, Vol. 55, No. 3, pp. 255-269.
- 8 Franke, K.W., Kramer, S.L. 2014. Procedure for the Empirical Evaluation of Lateral Spread Displacement Hazard Curves. *Journal of Geotechnical and Geoenvironmental Engineering*, Vol. 140, No. 1, pp. 110-120.
- 9 Greef, J. de, Lengkeek, H.J. 2018. Transition- and thin layer corrections for CPT based liquefaction analysis. *Cone Penetration Testing 2018 - Papers*, pp. 317-322.
- 10 Green, R.A. 2018. Groningen-Specific Liquefaction Evaluation - Summary (background document to the 2018 version of the NPR9998).
- 11 Green, R.A., Bommer, J.J., Stafford, P.J., Maurer, B.W., Edwards, B., Kruiver, P.P., Rodriguez-Marek, A., Lange, G. de, Oates, S.J., Storck, T., Omid, P., Bourne, S.J., Elk, J. van. 2018. Liquefaction Hazard Pilot Study for the Groningen Region of the Netherlands due to Induced Seismicity. <https://www.nam.nl/feiten-en-cijfers/onderzoeksrapporten>.
- 12 Green, R.A., Bommer, J.J. 2019. What is the Smallest Earthquake Magnitude that Needs to be Considered in Assessing Liquefaction Hazard? *Earthquake Spectra*, Vol. 35(3), pp. 1441-1464.
- 13 Hamada, M., Towhata, I., Yasuda, S., Isoyama, R. 1987. Study on permanent ground displacement induced by seismic liquefaction. *Computers and Geotechnics* 4, pp. 197-220.
- 14 Hamada, M., O'Rourke, T.D. 1992. Case Studies of Liquefaction and Lifeline Performance During Past Earthquakes - Volume 1 Japanese case Studies. Technical Report NCEER-92-0001.
- 15 Hamada, M. 1999. Similitude law for liquefied-ground flow. *Proceedings of the Seventh US-Japan Workshop on Earthquake Resistant Design of Lifeline Facilities and Countermeasures Against Soil Liquefaction*, Technical Report MCEER-99-0019, pp. 191-205.
- 16 Idriss, I.M., Boulanger, R.W. 2008. Soil Liquefaction During Earthquakes. EERI Monograph MNO-12.
- 17 Ishihara, K. 1985. Stability of natural deposits during earthquakes. *Proceedings of the 11<sup>th</sup> International Conference on Soil Mechanics and Foundation Engineering*, pp. 321-376.
- 18 Korff, M., Lange, G. de, Meijers, P., Wiersma, A., Kloosterman, F. 2016. Liquefaction sensitivity of the shallow subsurface of Groningen. <https://www.nam.nl/feiten-en-cijfers/onderzoeksrapporten>.
- 19 Kramer, S.L. 1996. *Geotechnical Earthquake Engineering*. Prentice-Hall civil engineering and engineering mechanics series. Prentice Hall, Upper Saddle River, New Jersey, USA.

- 20 Kramer, S.L. 2013. Lateral Spreading. In: Bobrowsky P.T. (eds) Encyclopedia of Natural Hazards. Encyclopedia of Earth Sciences Series. Springer, Dordrecht.
- 21 Lange, D. de. 2018. CPT in Thinly Layered Soils - Validation Tests and Analysis for Multi Thin layer Correction. <https://www.nam.nl/feiten-en-cijfers/onderzoeksrapporten>
- 22 Olson, S.M., Stark, T.D. 2002. Liquefied strength ratio from liquefaction flow failure case histories. Canadian Geotechnical Journal, Vol. 39, pp. 629-647.
- 23 O'Rourke, M.J., Liu, X. 2012. Seismic Design of Buried and Offshore Pipelines - MCEER-12-MN04.
- 24 NEN. 2018. NPR9998 - Assessment of structural safety of buildings in case of erection, reconstruction and disapproval - Induced earthquakes - Basis of design, actions and resistances (in Dutch).
- 25 Rauch, A.F. 1997. EPOLLS: An Empirical Method for Predicting Surface Displacements Due to Liquefaction-Induced Lateral Spreading in Earthquakes (PhD thesis), Blacksburg, Virginia, USA.
- 26 Vaid, Y.P., Chern, J.C. 1983. Effect of Static Shear on Resistance to Liquefaction. Soils and Foundations, Vol. 23, No. 1, pp. 47-60.
- 27 Valsamis, A.I., Bouckovalas, G.D., Papadimitriou, A.G. 2010. Parametric investigation of lateral spreading of gently sloping liquefied ground. Soil Dynamics and Earthquake Engineering 30, pp. 490-508.
- 28 WL | Delft Hydraulics. 2002. Invloed van aardbevingen op overstromingsrisico's.
- 29 Youd, T.L. 1973. Liquefaction, Flow and Associated Ground Failure. Geological Survey Circular 688.
- 30 Youd, T.L., Hansen, C.M., Bartlett, S.F. 2002. Revised Multilinear Regression Equations for Prediction of Lateral Spread Displacement. Journal of Geotechnical and Geoenvironmental Engineering, Vol. 128, No. 12, pp. 1007-1017.
- 31 Youd T.L., DeDen, D.W., Bray, J.D., Sancio, R., Cetin, K.O., Gerber, T.M. 2009. Zero-Displacement Lateral Spreads, 1999 Kocaeli, Turkey, Earthquake. Journal of Geotechnical and Geoenvironmental Engineering, Vol. 135, No. 1, pp. 46-61.
- 32 Youd, T.L. 2018. Application of MLR Procedure for Prediction of Liquefaction-Induced Lateral spread displacement. Journal of Geotechnical and Geoenvironmental Engineering, Vol. 144, Issue 6.
- 33 Zhang, J., Zhao, J.X. 2005. Empirical models for estimating liquefaction-induced lateral spread displacement. Soil Dynamics and Earthquake Engineering 25, pp. 439-450.
- 34 Zhang, G., Robertson, P.K., Brachman, R.W.I. 2004. Estimating Liquefaction-Induced Lateral Displacements Using the Standard Penetration Test of Cone Penetration Test. Journal of Geotechnical and Geoenvironmental Engineering, Vol. 130, No. 8, pp. 861-871.

